Supplemental information

Trigger inducible tertiary lymphoid structure formation using covalent organic frameworks for cancer immunotherapy

Liang Zhang[1,2,#], Boxin Zhang[1,#], Meng-Jie Zhang[1,#], Wenlang Li[2], Hao Li[1], Yantian Jiao[2], Qi-Chao Yang[1], Shuo Wang[1], Yuan-Tong Liu[1], An Song[1], Hai-Tao Feng[4], Jianwei Sun[2], Ryan T. K. Kwok[2], Jacky W. Y. Lam[2*], Ben Zhong Tang[2,3*], Zhi-Jun Sun[1*]

[1] State Key Laboratory of Oral & Maxillofacial Reconstruction and Regeneration, Key Laboratory of Oral Biomedicine Ministry of Education, Hubei Key Laboratory of Stomatology, School & Hospital of Stomatology, Frontier Science Center for Immunology and Metabolism, Taikang Center for Life and Medical Sciences, Wuhan University, Wuhan, 430079, China.

[2] Department of Chemistry, The Hong Kong Branch of Chinese National Engineering Research Center for Tissue Restoration and Reconstruction, Division of Life Science and State Key Laboratory of Molecular Neuroscience, The Hong Kong University of Science and Technology, Clear Water Bay, Kowloon, Hong Kong, 999077, China.

[3] Shenzhen Institute of Aggregate Science and Technology, School of Science and Engineering, The Chinese University of Hong Kong, Shenzhen, Guangdong 518172, China.

[4] AIE Research Center, College of Chemistry and Chemical Engineering, Baoji University of Arts and Sciences, Baoji, Shanxi, 721013, China.

[#] These authors contributed equally: Liang Zhang, Boxin Zhang, Meng-Jie Zhang.
[*]email: chjacky@ust.hk; tangbenz@cuhk.edu.cn; sunzj@whu.edu.cn

Experimental Section

***Chemicals*:** The organic solvent utilized in this study was obtained from Adamas-beta®. The fluorescent dyes, namely 2,7-dichloro-dichlorofluorescein diacetate (DCFH-DA), AIEgens-based monomers including 4',5'-bis(4-aminophenyl)-[1,1':2',1''-terphenyl]-4,4''-diamine (M-TPDA), 4,4',4'',4'''-([1,1'-biphenyl]-4,4'-diylbis(azanetriyl))-tetrabenzaldehyde (M-TDTA), 4,4',4'',4'''-((benzo[c]-[1,2,5]thiadiazole-4,7-diylbis(4,1-phenylene))bis(azanetriyl))tetrabenzaldehyde (M-BT), and 4,4',4'',4'''-((((1E,1'E)-benzo[c][1,2,5]thiadiazole-4,7-diylbis(ethene-2,1-diyl))bis(4,1-phenylene)-bis-(azanetriyl))tetrabenzaldehyde (M-ViBT) were purchased from Shanghai Kylpharm Co., Ltd and Jilin Chinese Academy of Sciences-Yanshen Technology Co., Ltd. The CCK8 reagent was acquired from Dojindo Laboratories (Japan), and the anti-mouse PD-1 mAb (CD279) and CTLA-4 were obtained from BioXcell (NH, USA).

***Instruments*:** Fluorescence spectra were acquired utilizing the Cary Eclipse Fluorescence Spectrophotometer (Agilent Technologies), while UV-vis absorption spectra were obtained using the Cary 300 UV-vis Spectrophotometer (Agilent Technologies). Size distribution and zeta potential measurements were conducted using the Zetasizer Nano-ZS90 (Malvern). X-ray photoelectron spectroscopy (XPS) measurements were recorded using the Thermal Fisher ESCALAB 250Xi instrument. TEM images were tested by a 200kV high-resolution transmission electron microscope (JEM-2100 Plus, JEOL, Japan).

***Synthesis of COF@PEG sample*:** The COF samples were effectively dispersed in a PBS solution utilizing F-127 as PEG generators. In detail, 50 mg of COF samples and 50 mg F-127 were dispersed in 100 ml of PBS and subjected to 24-hour sonication using an 1800 W ultrasonic cell shredder (JY99-IIDN, from Ningbo Scientz Biotechnology Co., Ltd, www.scientz.com). The obtained mixture was then subjected to centrifugation at 2500 rpm for 30 min to eliminate un-isolated nanoparticles, followed by centrifugation at 8000 rpm for 15 min to yield the isolated COF@PEG samples.

***FT-IR spectra for ligands and COFs*:** The IR spectra were obtained utilizing a Thermo Nicolet iS10 IR spectroscopy instrument manufactured by Thermo Fisher. The samples were tableted and the KBr background was employed. The wavelength range was set to 3700 to 600 cm^{-1}. The

successful formation of the imine linkage was confirmed by the appearance of a peak at approximately 1620 cm^{-1} in the Fourier transform infrared (FT-IR) spectrum, which corresponds to the telescopic vibration of the imine bond ($\nu_{C=N}$).

***X-ray Photoelectron Spectrometer (XPS) measurement*:** X-ray photoelectron spectroscopy (XPS) was conducted utilizing a Thermo Fisher ESCALAB 250Xi spectrometer, with the ion source of Al Kα, and the samples were prepared in a tablet form for the analysis. The XPS spectra exhibited the alteration in the chemical environment of nitrogen before and after the conversion to COFs. The emergence of new N 1s peaks at 398.8 eV confirmed the successful formation of imine bonds.

***UV-Vis diffuse reflectance spectra for ligands and COFs*:** The UV-vis diffuse reflectance spectra (UV-vis DRS) of COFs were acquired using a PerkinElmer Lambda 750 S spectroscopy instrument with $BaSO_4$ as the background. The band gap calculations were determined through the Kubleka-Munk theory. The optical absorption coefficient (α) was computed from the reflectance data using the Kubelka-Munk equation, in which $F(R) = \alpha = (1-R)^2/2R$, where R signifies the percentage of reflected light. The transformed Kubelka-Munk function, $[F(R)h\nu]^2 = A(h\nu-Eg)$, where Eg is the band gap energy, A is the constant dependent on transition probability, and intercept of $[F(R)h\nu]^2$ vs hν is Eg, relates the incident photon energy (hν) and the optical band gap energy (Eg). In comparison with the corresponding molecular building blocks, the COFs demonstrated smaller band gaps.

***N_2 adsorption analysis of these COFs*:** The N_2 adsorption isotherms were acquired utilizing a Quantachrome Autosorb-IQ2 automatic volumetric instrument in a liquid nitrogen bath (77 K), with ultra-high purity grade N_2 utilized for the adsorption experiments. The BET surface area analysis was carried out by plotting $x/v(1 - x)$ versus x, where $x = P/P_0$ (P_0 = 1 bar) and v represents the volume of nitrogen adsorbed per gram of COF at standard temperature and pressure (STP), and satisfactory correlation coefficients and positive C constant were observed. The linear region between the dashed lines provides the slope ($[c - 1]/v_{mc}$) and y-intercept ($1/v_{mc}$), which give the monolayer capacity, v_m, utilized to determine the surface area via $A = v_m\sigma_0N_{AV}$, where σ_0 is the cross-section area of the adsorbate at liquid density (16.2 $Å^2$ for nitrogen) and N_{AV} is Avogadro's

number. The surface areas of the TPDA-TDTA-COF, TPDA-BT-COF, and TPDA-ViBT-COF were determined to be 1040, 1230, and 1610 $m^2 g^{-1}$, respectively.

***Determine the crystal structure of these COFs*:** A 9 KW lab-based diffractometer was operated at 45 kV, 200 mA using Cu Kα (λ = 1.5418 Å) with a scan speed of 1 °/min and a step size of 0.01º in 2θ at ambient temperature and pressure utilized for powder X-ray diffraction (PXRD) characterization. Structure models for TPDA-TDTA-COF, TPDA-BT-COF, and TPDA-ViBT-COF were generated using the Materials Studio (ver. 8.0) suite of programs. Reflex, a software package for crystal determination from PXRD patterns, was employed for Pawley refinement. The unit cell dimension was set to the theoretical parameters, and the lattice parameters were iteratively optimized through Pawley refinement until the Rwp and Rp values converged, and the overlay of the observed with refined profiles displayed good agreement. The lattice models were fully optimized using the MS Forcite molecular dynamics module method for each COF model. The Reflex Plus module of the Material Studio was used for Pawley refinement, which exhibited good agreement with the experimental PXRD patterns. The (Rwp, Rp) values were (2.96%, 2.12%) for TPDA-TDTA-COF, (2.60%, 2.03%) for TPDA-BT-COF, and (1.96%, 1.46%) for TPDA-ViBT-COF, with Pawley refined cell parameters of a = 26.75 Å, b = 23.15 Å, c = 3.64 Å and α = β = γ = 90° for TPDA-TDTA-COF, a = 27.70 Å, b = 23.63 Å, c = 3.80 Å, α = β = γ = 90° for TPDA-BT-COF, and a = 29.52 Å, b = 22.70 Å, c = 3.74 Å, α = β = γ = 90° for TPDA-ViBT-COF.

***Solid-State NMR Experiments for COFs*:** High-resolution solid-state nuclear magnetic resonance (ssNMR) spectra were carried out on a Bruker Advance 400 MHz spectrometer using a 4 mm double resonance magic angles pinning (MAS) probe under a spinning speed of 10.0 kHz. The cross-polarization (CP) contact time was set to 3.0 ms for ^{13}C detection. 20000~24000 scans were accumulated for the $^{1}H^{13}C$ CP/MAS NMR experiments. ^{13}C chemical shifts were referenced to the adamantane CH_2 signal at 38.5 ppm.

***DFT calculations*:** Two fragments of TPy-imine COF and TPy-vinyl COF were fully optimized with the density functional theory (DFT) method by using B3LYP density functional and 6-31G(d,p) basis set. Analytical frequency calculations were also performed at the same level of

theory to confirm that the optimized structures were at a minimum point. The above quantum chemical calculations were carried out by using Gaussian 16, Revision A.03.

ScRNA-seq: 1×10^6 MC38 cells were inoculated in the right blank C57BL/6 mouse to establish MC38-tumor-bearing mice. Following an eight-day post-injection period, the mice were randomly distributed among two groups with varying treatments (Control, 660 nm laser (1.0 W cm^{-2}, 5 min) and TPDA-ViBT-COF+660 nm laser (1.0 W cm^{-2}, 5 min). On day 15 post-phototherapy, the C57BL/6 mice were euthanized, and the tumors were harvested. The tumors were then processed into single-cell suspensions, with a cell concentration of 700-1200 cells μL^{-1} for each sample for ScRNA-seq. The MobiCube Single-Cell 3' RNA-seq Kit v1.0 (MobiDrop) was used to prepare the library, which was subsequently sequenced using Illumina NovaSeq 6000 Systems. Normalized aggregate data was generated across the samples using the MobiVision software pipeline (version 1.1, MobiDrop). This process involved demultiplexing cellular barcodes, mapping reads to the genome and transcriptome using STAR solo, and down-sampling reads as needed. The resulting output data yielded a matrix of gene counts versus cells.

***ScRNA-seq data processing*:** The scRNA-seq data were processed with the Seurat (v4.3.0.1) package in R software. Cells with fewer than 200 genes detected or >10% mitochondrial UMI counts were dropped out. After quality control, a total of 17182 cells were obtained for downstream analysis. For total-count correction, the normalized date matrix was obtained by the total expression and multiplied by a scale factor (10,000 by default). The highly variable genes matrix was generated by the Find Variable Features function of the Seurat package. The top 2000 highly variable features were extracted for further analysis. Based on these highly variable genes, the principal component analysis was performed. The first 50 principal components were extracted for UMAP dimensionality reduction and the cell populations were identified by graph-based clustering using canonical marker genes' average expression.

In vivo antitumor effects in 4MOSC1-tumor-bearing mice: To establish 4MOSC1-tumor-bearing mice animal model, a total of 2×10^6 4MOSC1 cells inoculated subcutaneously into the right back of C57BL/6 mice. The antitumor efficacy of AIE COFs was evaluated using the 4MOSC1-tumor-bearing mouse animal model. Following an eight-day post-injection period, the mice were

randomly distributed among six groups with varying treatments (Control, 660 nm laser (1.0 W cm^{-2}, 5 min), TPDA-TDTA-COF, TPDA-TDTA-COF+660 nm (1.0 W cm^{-2}, 5 min), TPDA-BT-COF+660 nm (1.0 W cm^{-2}, 5 min), and TPDA-ViBT-COF+660 nm laser (1.0 W cm^{-2}, 5 min). AIE COFs in a dose of 5 mg kg^{-1} were administered to each group (intratumoral injection), and body weights and tumor volumes were monitored every three days.

***Photothermal imaging in vivo*:** To monitor the photothermal capability of TPDA-ViBT-COF in vivo, MC38 tumor-bearing mice were utilized for in vivo photothermal imaging. When the tumor volume reached ~200 mm^3, TPDA-ViBT-COF was intratumorally injected into the mice at the dose of 5mg kg^{-1}. After 24 h injection, we irradiated the tumor with a 660 nm laser with a power of 1.0 W cm^{-2} for 5 min. The photothermal images of mice were obtained by an infrared camera every minute.

***Tumor rechallenge*:** To test the immune memory of TPDA-ViBT-COF+αCTLA4 curing mice. When the tumor volume exceeded 100 mm^3, TPDA-ViBT-COF+αCTLA4 combination therapy was administered. After 40 days, 3×10^5 MC38-luc cells were subcutaneously inoculated on the left backs of both the treated group and the healthy mice for comparison. The tumor volume was monitored every two days and the tumor was visualization by using Fluorescein imaging.

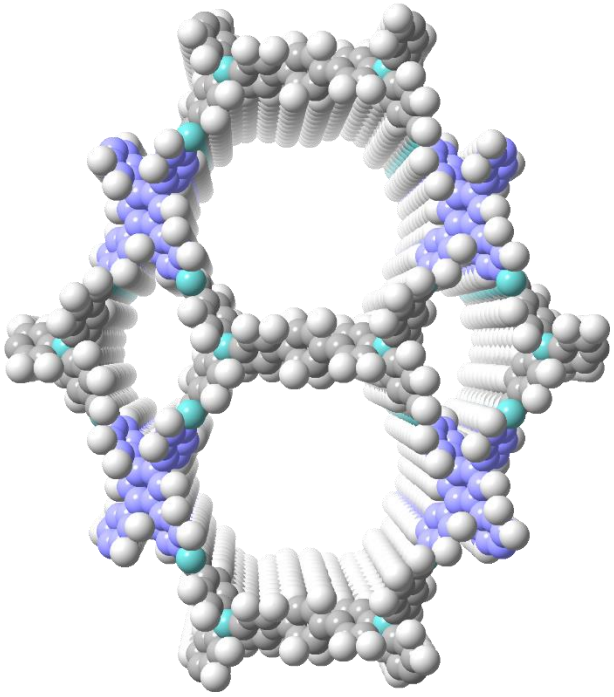

Supplementary Fig. 1. Space-filling models of TPDA-TDTA-COF from the top view.

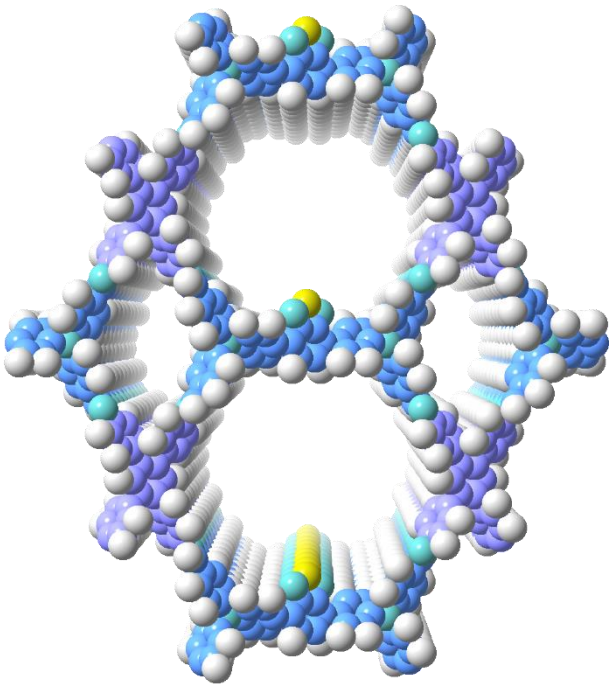

Supplementary Fig. 2. Space-filling models of TPDA-BT-COF from the top view.

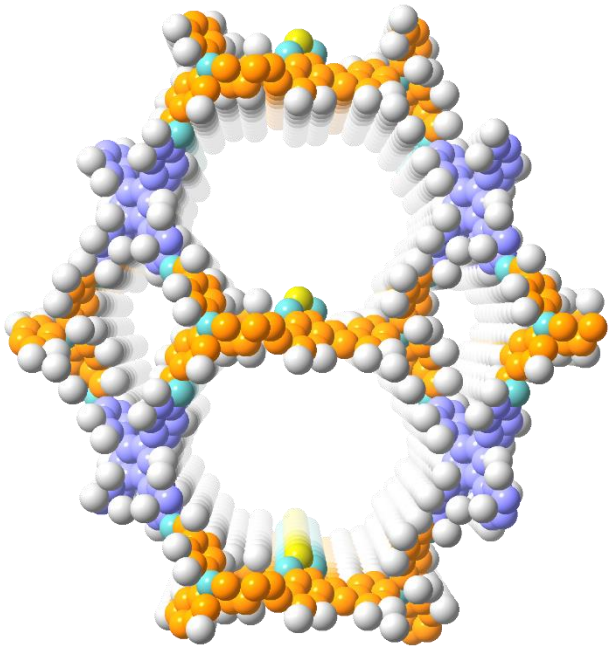

Supplementary Fig. 3. Space-filling models of TPDA-ViBT-COF from the top view.

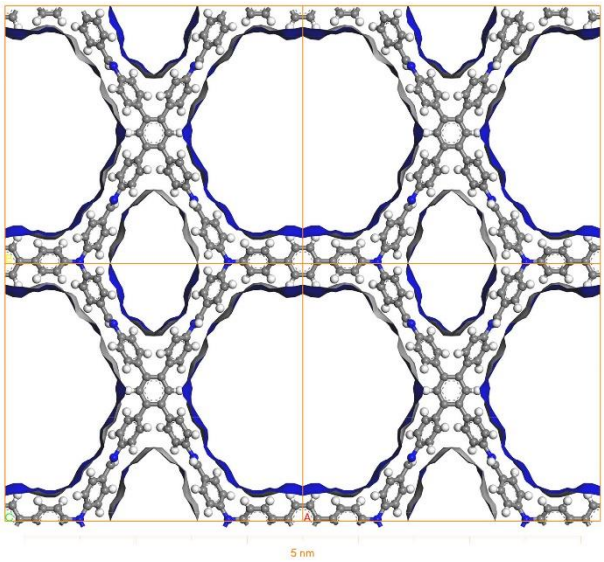

Supplementary Fig. 4. Connolly surface of TPDA-TDTA-COF, with surface area value of 382.98 $Å^2$, carbon, hydrogen, and nitrogen atoms are represented as grey, white, and blue spheres, respectively.

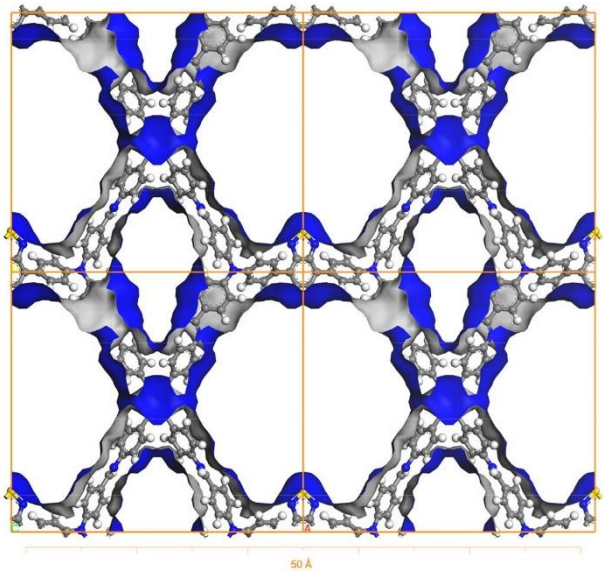

Supplementary Fig. 5. Connolly surface of TPDA-BT-COF, with surface area value of 703.52 $Å^2$, carbon, hydrogen, and nitrogen atoms are represented as grey, white, and blue spheres, respectively.

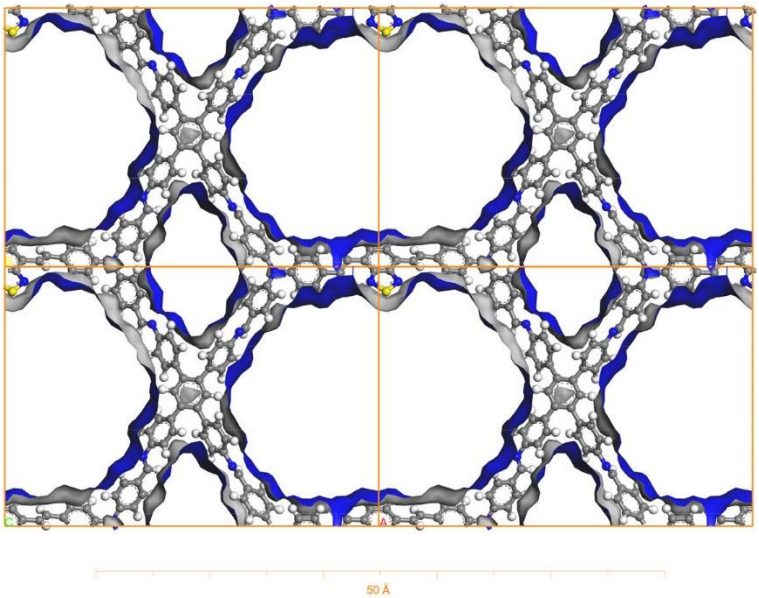

Supplementary Fig. 6. Connolly surface of TPDA-ViBT-COF, with surface area value of 653.36 $Å^2$, carbon, hydrogen, and nitrogen atoms are represented as grey, white, and blue spheres, respectively.

Supplementary Table 1. Crystallographic Information of Modeled COFs.

	TPDA-TDTA-COF	**TPDA-BT-COF**	**TPDA-ViBT-COF**
Space group	*P*2	*P*2	*P*2
***a* (Å)**	26.75	27.70	29.52
***b* (Å)**	23.15	23.63	22.70
***c* (Å)**	3.64	3.80	3.74
R_p **(%)**	2.96	2.60	1.96
R_{wp}**(%)**	2.12	2.03	1.46
α **(°)**	90	90	90
β **(°)**	90	90	90
γ **(°)**	90	90	90

Supplementary Table 2. Atomic parameters of TPDA-TDTA-COF.

Atomic parameters of TPDA-TDTA-COF							
Atom	*x* (Å)	*y* (Å)	*z* (Å)	Atom	*x* (Å)	*y* (Å)	*z* (Å)
C1	0.60718	0.29815	1.4747	C36	2.44715	1.61349	0.53396
C2	0.89844	0.00881	1.51406	C37	2.45298	1.65579	0.33877
C3	0.87247	0.04822	0.67546	C38	2.42576	1.70576	0.34995
C4	0.82374	0.04795	1.68667	H39	0.88981	0.07848	0.79717
C5	0.79998	0.00799	1.53846	H40	0.80452	0.07815	1.81519
C6	0.82589	-0.03118	1.37635	H41	0.80835	-0.06215	1.25959
C7	0.8746	-0.03062	1.36313	H42	0.89364	-0.06087	1.23377
C8	0.72573	-0.04852	1.57265	H43	0.68118	-0.02893	1.26403
C9	0.72309	0.05908	1.57786	H44	0.64101	-0.12251	1.28384
C10	0.69064	-0.06067	1.40485	H45	0.7221	-0.17424	1.92039
C11	0.66789	-0.1141	1.41629	H46	0.76382	-0.08129	1.88905
C12	0.67896	-0.15555	1.60214	H47	0.75748	0.09816	1.23197
C13	0.7134	-0.14302	1.77393	H48	0.71269	0.18892	1.27318
C14	0.73713	-0.0902	1.75655	H49	0.63909	0.1244	1.97946
C15	0.73149	0.10365	1.39424	H50	0.68232	0.03318	1.9289
C16	0.70596	0.15518	1.41795	H51	1.95599	0.9146	0.50983
C17	0.67263	0.1633	1.63013	H52	2.3494	0.76767	0.18503
C18	0.66469	0.119	1.81477	H53	2.36067	1.33524	0.19419
C19	0.68918	0.06698	1.78619	H54	2.40829	1.42371	0.18034
N20	0.74967	0.00626	1.55679	H55	2.4777	1.36339	0.84304
C21	0.35414	0.21738	-0.6624	H56	2.43077	1.27481	0.85715
N22	0.36551	0.24621	-0.4593	H57	2.36026	1.67854	0.91845
C23	1.95016	1.00815	0.5061	H58	2.40808	1.58996	0.89652
C24	1.97561	1.06012	0.5031	H59	2.47841	1.64973	0.17704
C25	1.97437	0.95552	0.50317	H60	2.43145	1.738	0.19747
C26	2.34651	0.78927	0.37347	C61	0.45136	0.50657	0.52108
N27	2.36412	0.76588	0.57473	C62	0.47526	0.45363	0.50592
C28	2.39179	0.71422	0.55789	C63	0.47525	0.55952	0.51553
C29	2.38661	1.34075	0.33491	H64	1.95764	1.10129	0.50292
C30	2.4135	1.39129	0.32818	H65	0.3675	0.23019	-0.85744
C31	2.4472	1.39966	0.50975	H66	0.41351	0.50657	0.53721
C32	2.45274	1.35724	0.70002				
C33	2.42571	1.30708	0.70872				
C34	2.38614	1.67246	0.75602				
C35	2.41325	1.62206	0.74286				

Supplementary Table 3. Atomic parameters of TPDA-BT-COF

Atomic parameters of TPDA-BT-COF							
Atom	*x* (Å)	*y* (Å)	*z* (Å)	Atom	*x* (Å)	*y* (Å)	*z* (Å)
C1	0.60718	0.29815	1.4747	C36	2.44715	1.61349	0.53396
C2	0.89844	0.00881	1.51406	C37	2.45298	1.65579	0.33877
C3	0.87247	0.04822	0.67546	C38	2.42576	1.70576	0.34995
C4	0.82374	0.04795	1.68667	H39	0.88981	0.07848	0.79717
C5	0.79998	0.00799	1.53846	H40	0.80452	0.07815	1.81519
C6	0.82589	-0.03118	1.37635	H41	0.80835	-0.06215	1.25959
C7	0.8746	-0.03062	1.36313	H42	0.89364	-0.06087	1.23377
C8	0.72573	-0.04852	1.57265	H43	0.68118	-0.02893	1.26403
C9	0.72309	0.05908	1.57786	H44	0.64101	-0.12251	1.28384
C10	0.69064	-0.06067	1.40485	H45	0.7221	-0.17424	1.92039
C11	0.66789	-0.1141	1.41629	H46	0.76382	-0.08129	1.88905
C12	0.67896	-0.15555	1.60214	H47	0.75748	0.09816	1.23197
C13	0.7134	-0.14302	1.77393	H48	0.71269	0.18892	1.27318
C14	0.73713	-0.0902	1.75655	H49	0.63909	0.1244	1.97946
C15	0.73149	0.10365	1.39424	H50	0.68232	0.03318	1.9289
C16	0.70596	0.15518	1.41795	H51	1.95599	0.9146	0.50983
C17	0.67263	0.1633	1.63013	H52	2.3494	0.76767	0.18503
C18	0.66469	0.119	1.81477	H53	2.36067	1.33524	0.19419
C19	0.68918	0.06698	1.78619	H54	2.40829	1.42371	0.18034
N20	0.74967	0.00626	1.55679	H55	2.4777	1.36339	0.84304
C21	0.35414	0.21738	-0.6624	H56	2.43077	1.27481	0.85715
N22	0.36551	0.24621	-0.4593	H57	2.36026	1.67854	0.91845
C23	1.95016	1.00815	0.5061	H58	2.40808	1.58996	0.89652
C24	1.97561	1.06012	0.5031	H59	2.47841	1.64973	0.17704
C25	1.97437	0.95552	0.50317	H60	2.43145	1.738	0.19747
C26	2.34651	0.78927	0.37347	C61	0.45136	0.50657	0.52108
N27	2.36412	0.76588	0.57473	C62	0.47526	0.45363	0.50592
C28	2.39179	0.71422	0.55789	C63	0.47525	0.55952	0.51553
C29	2.38661	1.34075	0.33491	H64	0.3675	0.23019	-0.85744
C30	2.4135	1.39129	0.32818	H65	0.41351	0.50657	0.53721
C31	2.4472	1.39966	0.50975	N66	0.96053	1.11772	0.50526
C32	2.45274	1.35724	0.70002	S67	1	1.15332	0.5
C33	2.42571	1.30708	0.70872				
C34	2.38614	1.67246	0.75602				
C35	2.41325	1.62206	0.74286				

Supplementary Table 4. Atomic parameters of TPDA-ViBT-COF

Atomic parameters of TPDA-ViBT-COF							
Atom	*x* (Å)	*y* (Å)	*z* (Å)	Atom	*x* (Å)	*y* (Å)	*z* (Å)
C1	0.60179	0.29187	0.38106	C37	0.44557	0.68283	0.92978
C2	0.85456	-0.01206	0.16242	C38	0.42092	0.73353	0.94898
C3	0.8272	0.04349	0.34617	H39	0.83898	0.08698	0.49349
C4	0.78376	0.04218	0.35636	H40	0.76305	0.08477	0.51052
C5	0.76697	-0.01452	0.1826	H41	0.78312	0.88738	-0.15865
C6	0.79503	0.93138	-0.01796	H42	0.85901	0.88924	-0.16868
C7	0.83832	0.93243	-0.02444	H43	0.6521	0.92655	0.02733
C8	0.70388	0.92575	0.24703	H44	0.6216	0.83442	0.0768
C9	0.69403	0.03411	0.26341	H45	0.72289	0.81288	0.48658
C10	0.66732	0.90321	0.13507	H46	0.75082	0.90936	0.47172
C11	0.65011	0.85016	0.15998	H47	0.73814	0.05905	-0.05694
C12	0.67013	0.81689	0.28439	H48	0.69244	0.14885	0.00819
C13	0.70724	0.8377	0.38712	H49	0.5959	0.11124	0.64925
C14	0.72323	0.89266	0.3774	H50	0.64276	0.02448	0.60153
C15	0.70737	0.07046	0.09976	H51	-0.01792	0.11305	0.29015
C16	0.68127	0.12171	0.13737	H52	0.33867	0.73307	0.40505
C17	0.64061	0.13636	0.33208	H53	0.36306	0.33891	0.52044
C18	0.62694	0.1001	0.49438	H54	0.4039	0.42247	0.45828
C19	0.65363	0.05023	0.46489	H55	0.49421	0.38751	0.92119
N20	0.72156	-0.01851	0.22633	H56	0.45568	0.29872	0.94875
C21	0.39729	0.20992	0.74571	H57	0.37429	0.64688	0.33234
N22	0.38212	0.26213	0.75552	H58	0.42123	0.56199	0.2981
C23	-0.03626	0.02855	0.34463	H59	0.46108	0.69109	1.11747
C24	-0.02215	-0.02022	0.40845	H60	0.42115	0.78048	1.13489
C25	-0.00825	0.07452	0.33729	C61	0.4558	0.51729	0.68269
C26	0.34695	0.77656	0.5783	C62	0.47846	0.46144	0.63319
N27	0.37394	0.77561	0.75568	C63	0.47596	0.56851	0.65619
C28	0.39549	0.72409	0.73669	H64	0.43119	0.19921	0.69942
C29	0.39212	0.34866	0.60349	H65	0.42152	0.52188	0.74813
C30	0.4154	0.39682	0.57134	N66	-0.04596	-0.06936	0.43687
C31	0.45356	0.41028	0.67414	C67	0.40682	0.31169	0.73115
C32	0.46666	0.3757	0.82143	C68	0.1607	0.04323	0.5447
C33	0.44443	0.32532	0.83945	C69	0.19399	0.07433	0.4527
C34	0.39453	0.65831	0.49647	C70	0.23487	0.06362	0.48264
C35	0.42169	0.60981	0.47415	C71	0.24288	0.02429	0.62217
C36	0.44853	0.62203	0.68227	C72	0.20893	0.99473	0.72285

Supplementary Table 4. Atomic parameters of TPDA-ViBT-COF (continue).

Atomic parameters of TPDA-ViBT-COF							
Atom	*x* (Å)	*y* (Å)	*z* (Å)	Atom	*x* (Å)	*y* (Å)	*z* (Å)
C73	0.16846	1.00345	0.68159	H107	0.2136	0.96505	0.83606
C74	0.29924	0.95446	0.64858	H108	0.14325	0.97934	0.75875
C75	0.31394	0.06412	0.70684	H109	0.33556	0.99697	1.00079
C76	0.32619	0.95313	0.83822	H110	0.36339	0.89642	0.96063
C77	0.34196	0.89556	0.8151	H111	0.29307	0.79474	0.25843
C78	0.32995	0.83779	0.60835	H112	0.26733	0.89561	0.28637
C79	0.3024	0.83874	0.42223	H113	0.26624	0.1419	1.01091
C80	0.28744	0.89643	0.44023	H114	0.3137	0.22565	1.03984
C81	0.29911	0.12856	0.88897	H115	0.41755	0.0833	0.46706
C82	0.32622	0.17636	0.90674	H116	0.36989	-0.00029	0.4232
C83	0.36902	0.16055	0.7515	H117	0.05378	0.10636	0.37839
C84	0.38458	0.09647	0.58732	H118	0.67295	0.72108	0.27054
C85	0.35729	0.04876	0.56275	H119	0.63693	0.35924	0.68688
N86	0.28509	0.01451	0.6621	H120	0.59234	0.45232	0.78055
C87	0.61222	0.18915	0.36847	H121	0.51758	0.3306	0.15767
N88	0.62764	0.23828	0.34027	H122	0.56116	0.23733	0.07807
C89	0.04581	0.02144	0.4545	H123	0.6169	0.6414	-0.00699
C90	0.01718	-0.02315	0.46346	H124	0.57517	0.55779	0.05622
C91	0.03272	0.07069	0.38811	H125	0.52748	0.68357	1.02317
C92	0.65204	0.76147	0.31439	H126	0.56221	0.7705	0.94641
N93	0.61175	0.76377	0.42274	C127	0.54368	0.50798	0.51822
C94	0.5916	0.7124	0.46374	C128	0.5235	0.45644	0.54545
C95	0.61082	0.35291	0.57147	C129	0.5208	0.56426	0.57684
C96	0.58535	0.40597	0.62371	H130	0.5783	0.18864	0.44128
C97	0.55091	0.39909	0.47984	H131	0.57794	0.50423	0.44912
C98	0.54325	0.33762	0.27617	N132	0.02447	-0.07473	0.53249
C99	0.56803	0.28432	0.23117	S133	-0.0182	-0.11749	0.52776
C100	0.59636	0.65127	0.2167	C134	0.89903	0.98427	0.18354
C101	0.57243	0.60374	0.25204	C135	0.92052	1.03467	0.30177
C102	0.54499	0.61571	0.5381	C136	1.08791	1.01527	0.5143
C103	0.5437	0.67525	0.79128	C137	1.11881	1.05159	0.48553
C104	0.56519	0.72407	0.75098	H107	0.2136	0.96505	0.83606
H105	0.18868	0.1051	0.34614				
H106	0.26028	0.08592	0.39498				

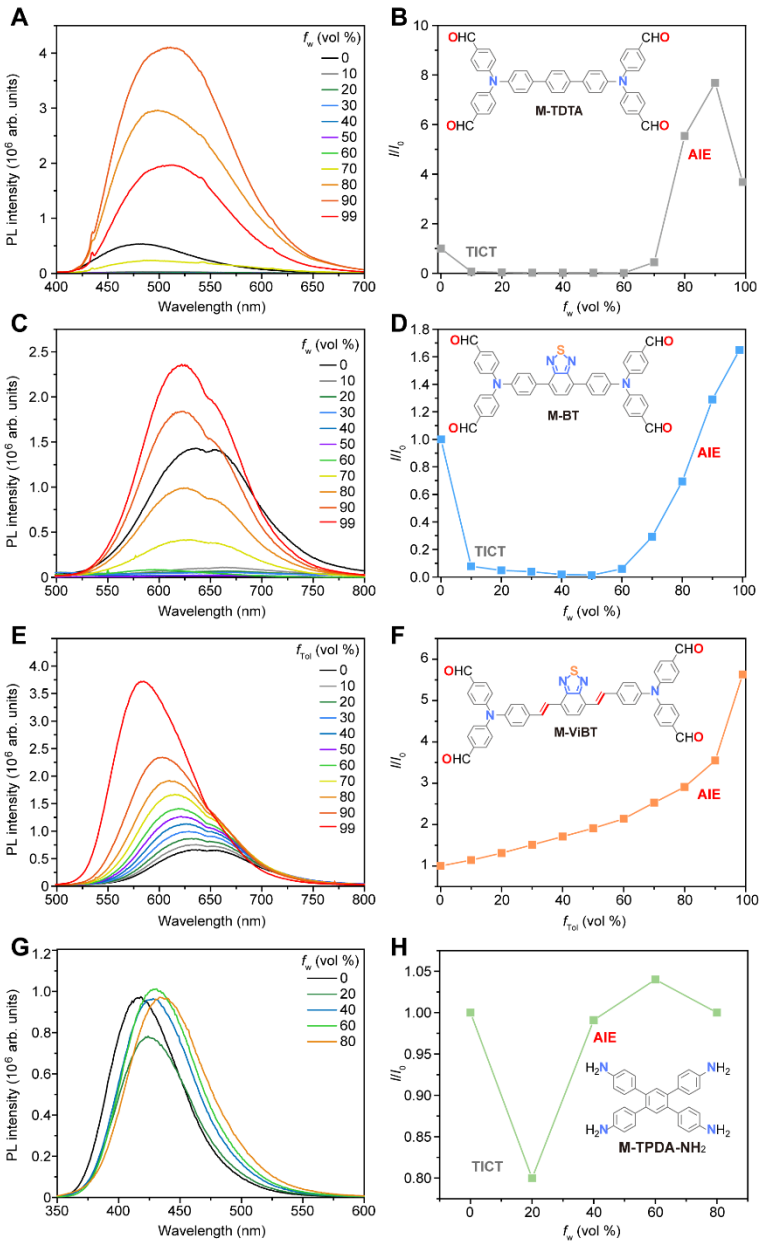

Supplementary Fig. 7. PL spectra of M-TPDA (A), M-TDTA (C), M-BT (E), and M-ViBT (G) in THF/H_2O solutions with different water fractions (f_w). Plots of the relative emission intensity (I/I_0) of M-TPDA (B), M-TDTA (D), M-BT (F), and M-ViBT (H) versus increased water fraction. Source data are provided as a Source Data file.

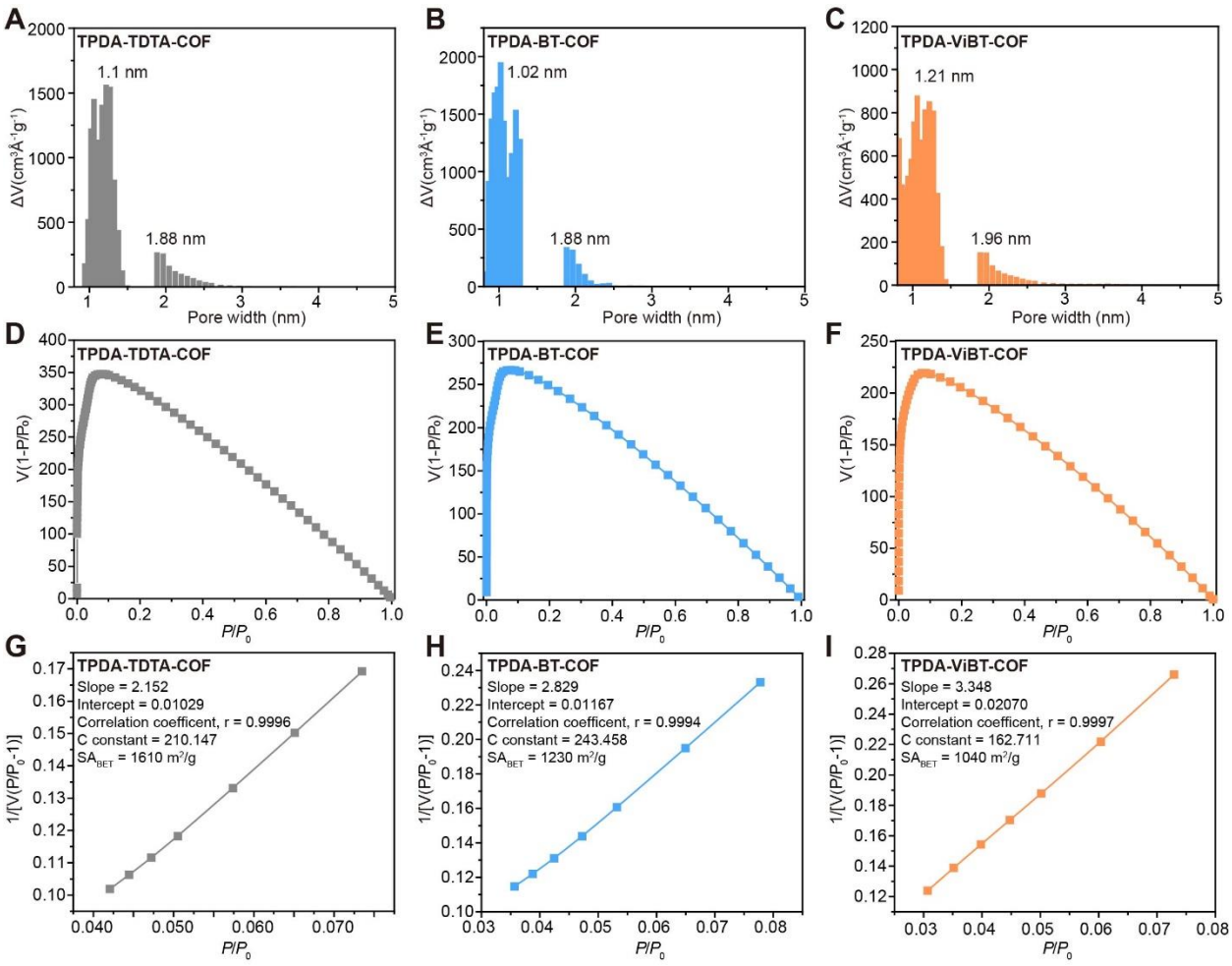

Supplementary Fig. 8. BET surface area was calculated for TPDA-TDTA-COF, TPDA-BT-COF and TPDA-ViBT-COF, based on nitrogen adsorption isotherm at 77 K. (A) to (C) pore size distribution of TPDA-TDTA-COF, TPDA-BT-COF and TPDA-ViBT-COF, (D) to (I) plot shows good fitting to the BET model. Source data are provided as a Source Data file.

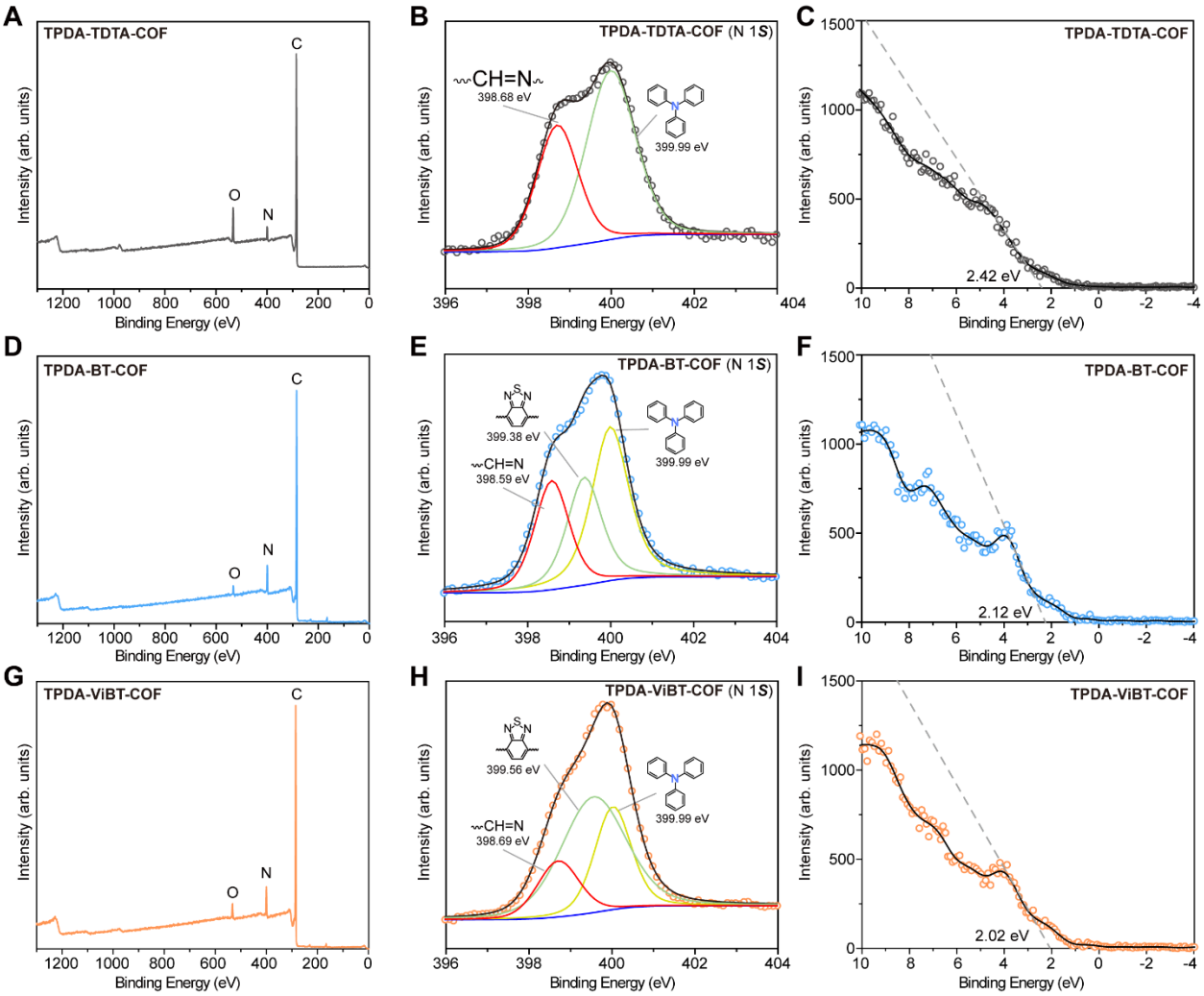

Supplementary Fig. 9. XPS spectra and valence band of TPDA-TDTA-COF, TPDA-BT-COF and TPDA-ViBT-COF. Source data are provided as a Source Data file.

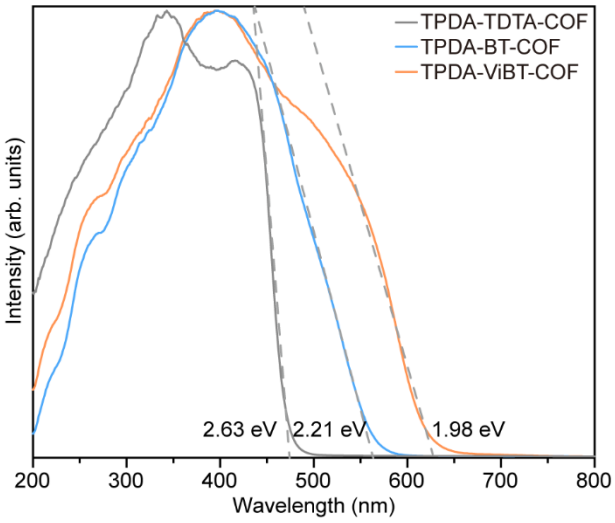

Supplementary Fig. 10. Solid state UV-Vis absorption property of TPDA-TDTA-COF, TPDA-BT-COF, and TPDA-ViBT-COF. Source data are provided as a Source Data file.

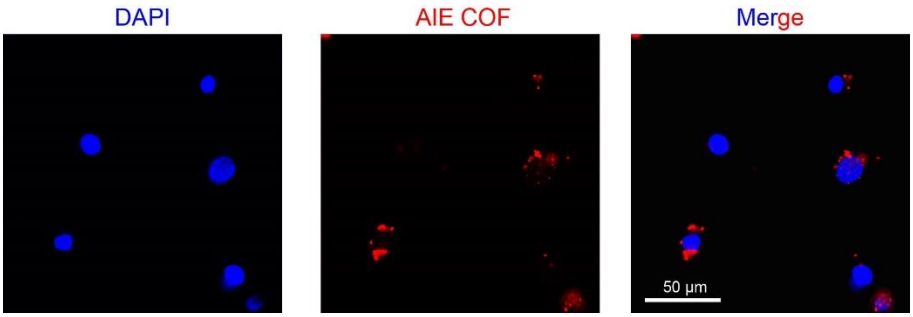

Supplementary Fig. 11. Intracellular uptake of AIE COF in MC38 cells, detected by confocal microscopy, scale bar = 50 μm. Data were repeated thrice independently with similar results.

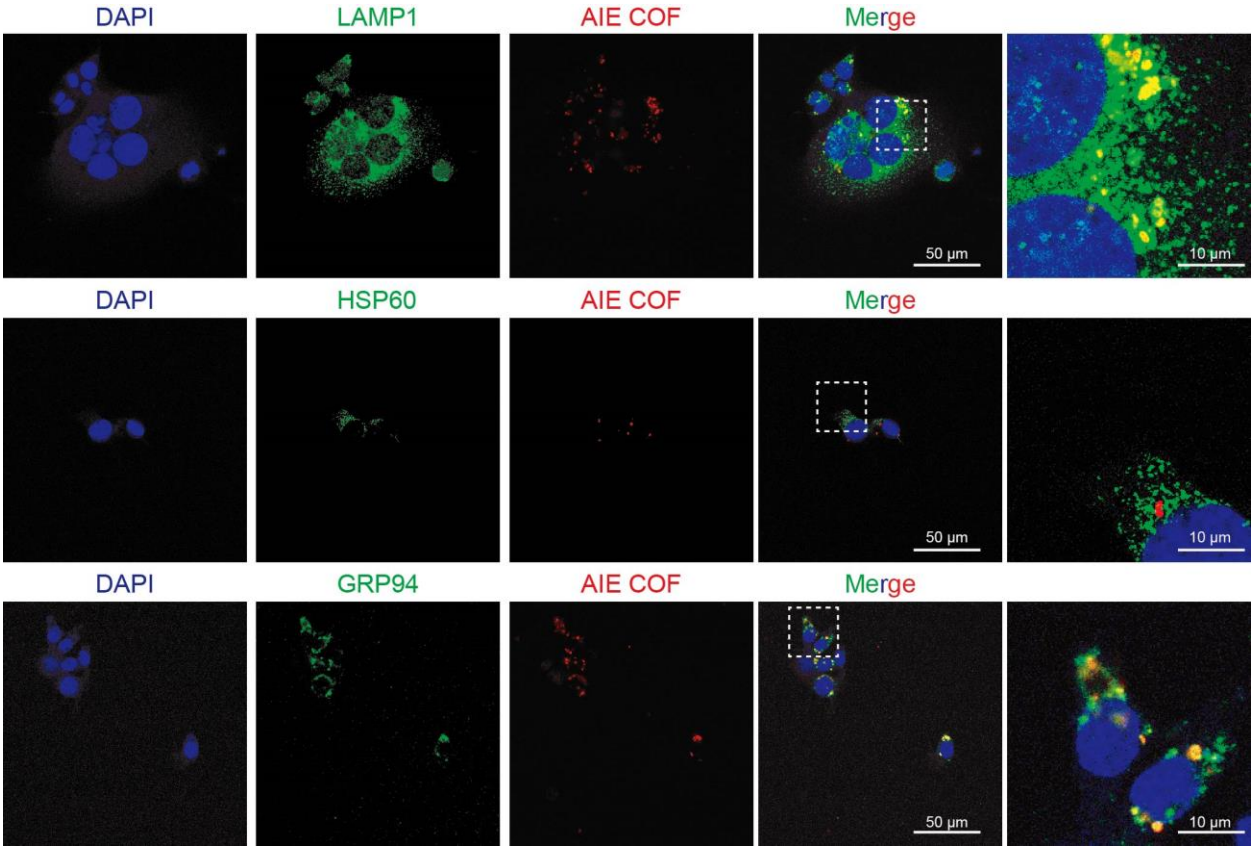

Supplementary Fig. 12. Subcellular distribution of AIE COF in MC38 cell, scale bar = 10 μm. Data were repeated thrice independently with similar results.

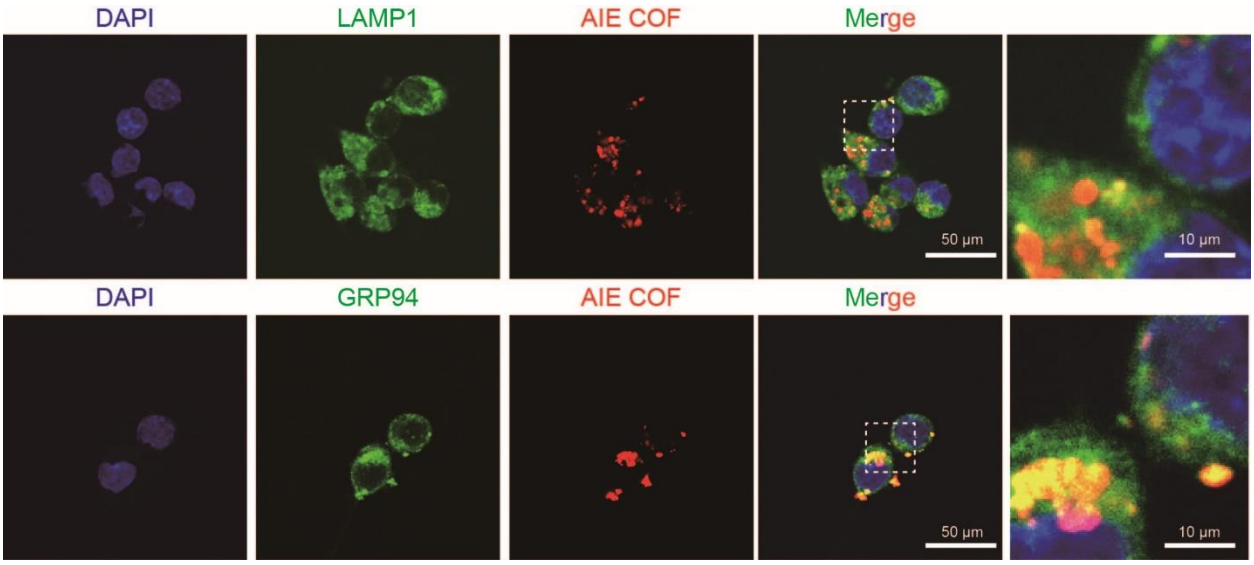

Supplementary Fig. 13. Subcellular distribution of AIE COF in RAW264.7 cell, scale bar = 10 μm. Data were repeated thrice independently with similar results.

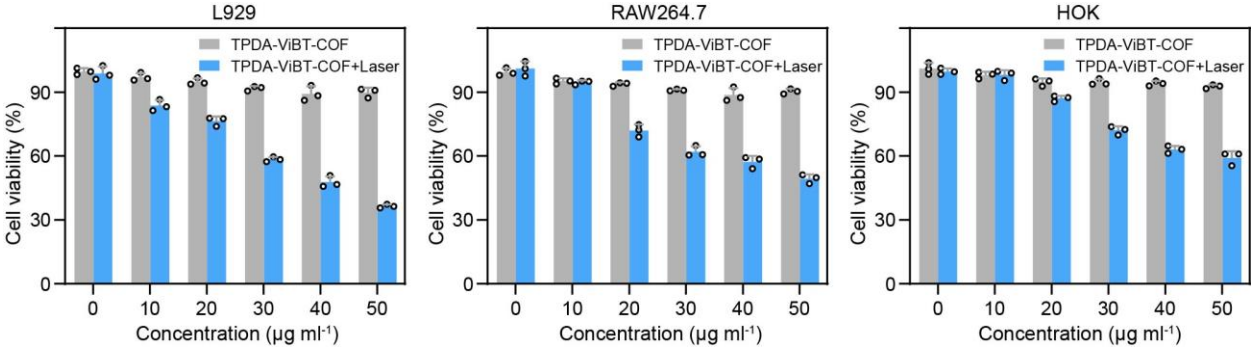

Supplementary Fig. 14. Cytotoxicity of TPDA-ViBT-COF without or upon 660 nm laser irradiation for L929, RAW264.7, and HOK cells. Source data are provided as a Source Data file. n = 3 independent samples.

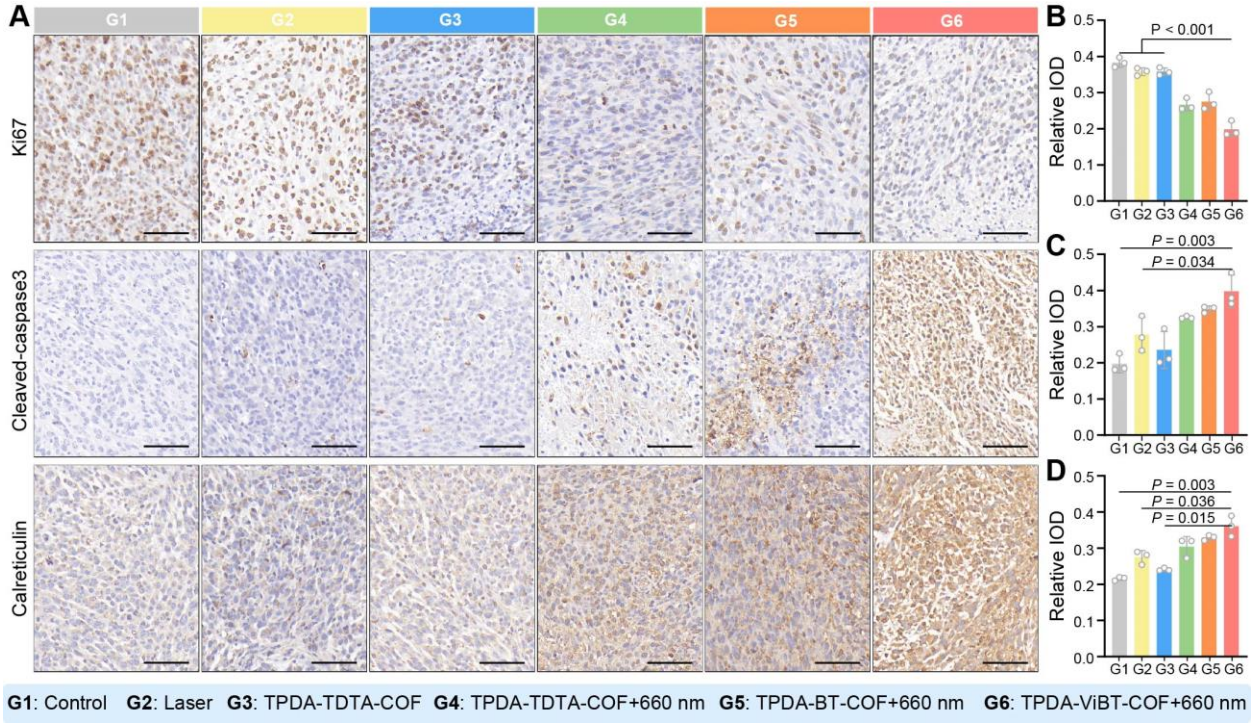

Supplementary Fig. 15. Quantification and representative immunohistochemical images of Ki67, Cleaved Caspase-3, and Calreticulin under different treatments, scale bar = 50 μm, n = 3 independent samples. (A) Representative immunohistochemical images of Ki67, Cleaved Caspase-3, and Calreticulin under different treatments, scale bar = 50 μm, n = 3 independent samples. (B) Quantification the immunohistochemical images of Ki67, Cleaved Caspase-3, and Calreticulin under different treatments, $P_{G(1\ vs\ 6)}$ = 0.0006, $P_{G(2\ vs\ 6)}$ = 0.0004, $P_{G(3\ vs\ 6)}$ = 1.65E-05. (C) Quantification the immunohistochemical images of Cleaved Caspase-3 under different treatments, $P_{G(1\ vs\ 6)}$ = 0.0008, $P_{G(2\ vs\ 6)}$ = 0.0001, $P_{G(3\ vs\ 6)}$ = 0.0004. (D) Quantification the immunohistochemical images of Calreticulin under different treatments, $P_{G(1\ vs\ 6)}$ = 0.0008, $P_{G(2\ vs\ 6)}$ = 0.0001, $P_{G(3\ vs\ 6)}$ = 0.0004. Data are presented as mean ± SEM, statistical significance was assessed using one-way ANOVA with post hoc Tukey test. Source data are provided as a Source Data file.

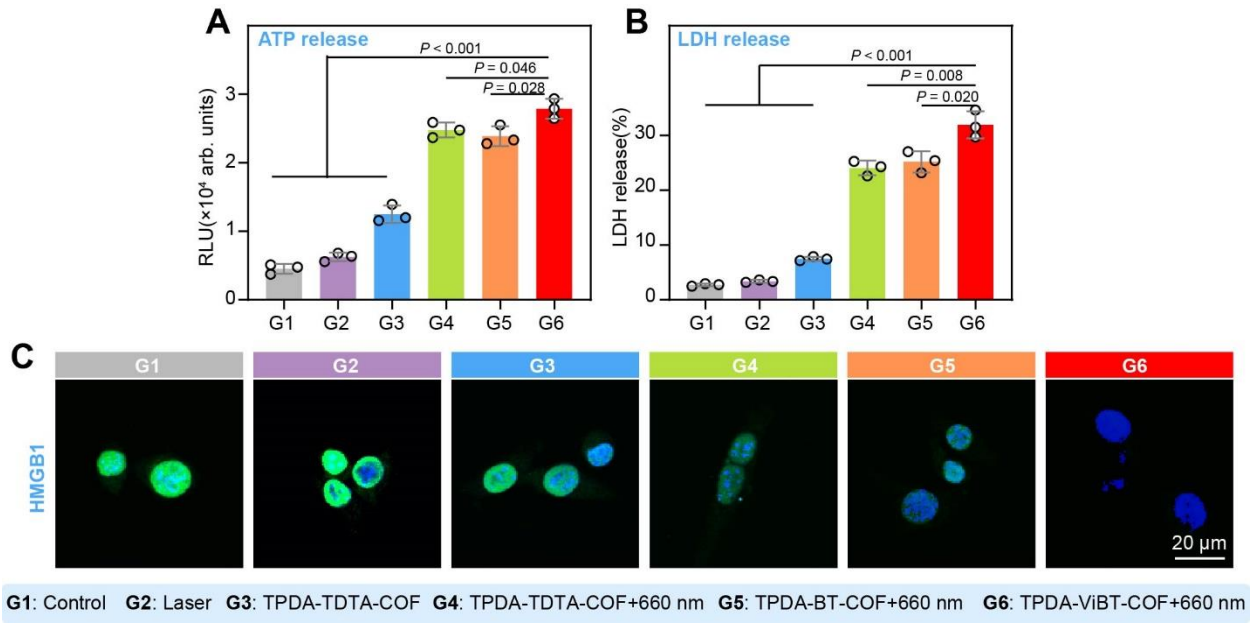

Supplementary Fig. 16. (A) ATP in MC38 cells after various treatments; data are presented as mean ± SEM (n = 3 independent samples), statistical significance was assessed using one-way ANOVA with post hoc Tukey test, $P_{G(1\ vs\ 6)}$ = 7.46 E -06, $P_{G(2\ vs\ 6)}$ = 9.06E-06, $P_{G(3\ vs\ 6)}$ = 7.72E-05. (B) LDH in MC38 cells after various treatments; data are presented as mean ± SEM (n = 3 independent samples), statistical significance was assessed using one-way ANOVA with post hoc Tukey test, $P_{G(1\ vs\ 6)}$ = 1.74 E -05, $P_{G(2\ vs\ 6)}$ = 1.91E-05, $P_{G(3\ vs\ 6)}$ = 3.61E-05. (C) Representative images of HMGB1 immunofluorescence staining in MC38 cells after treatment with different samples, three repeats are performed independently. Source data are provided as a Source Data file, scale bar = 20 μm.

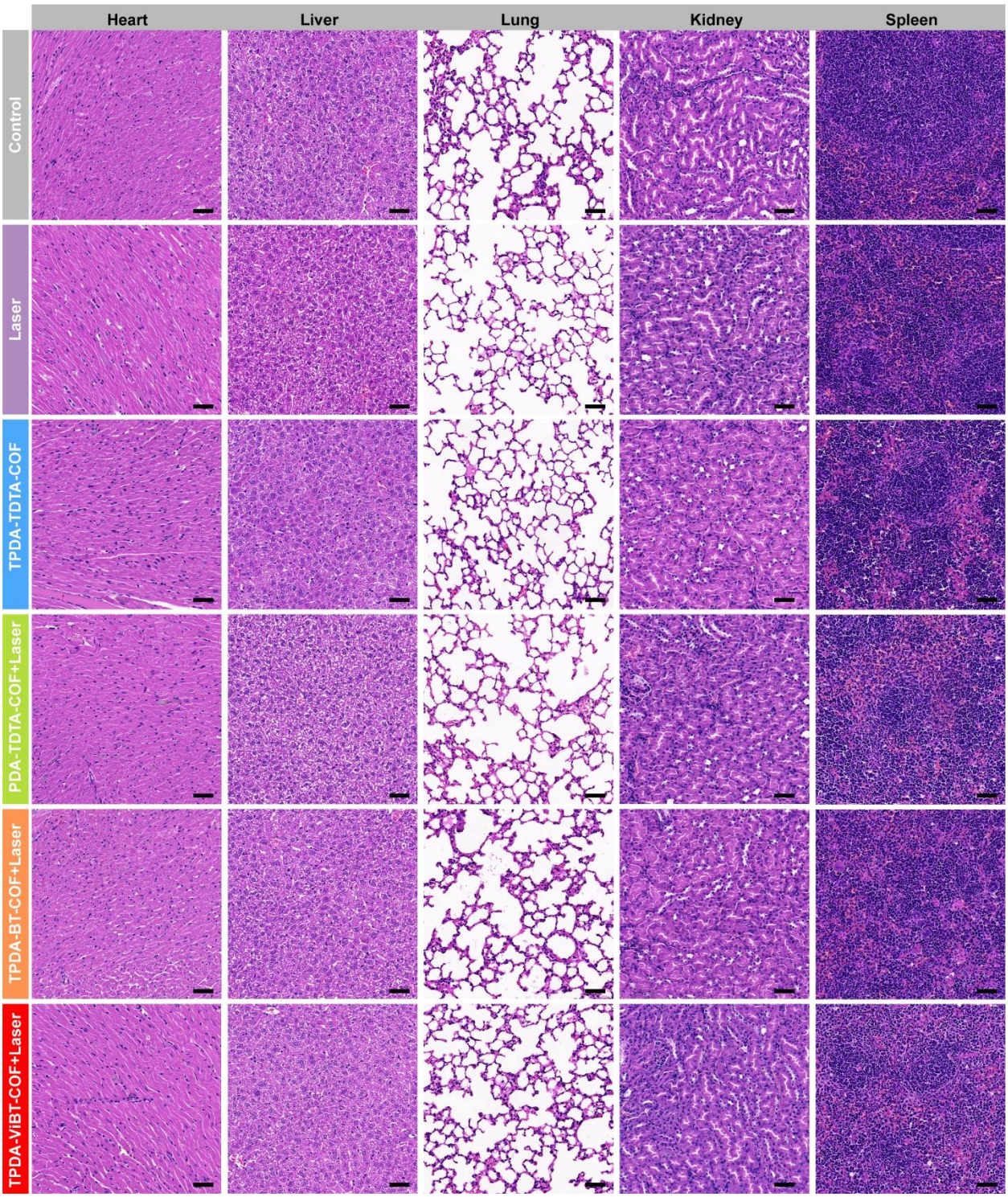

Supplementary Fig. 17. Representative H&E staining of major organs of differently treated mice, including hearts, livers, lungs, kidneys, and spleens, scale bar = 50 μm. Data were repeated thrice independently with similar results.

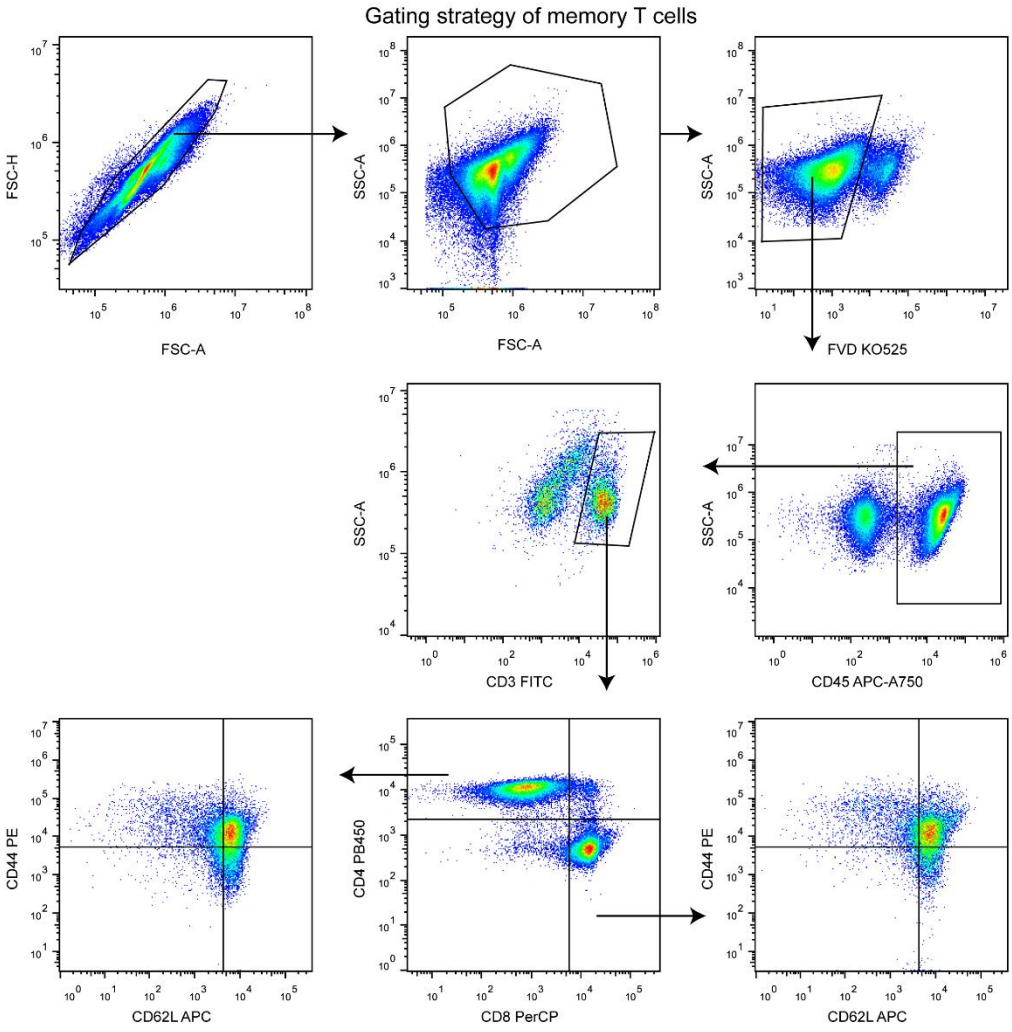

Supplementary Fig. 18. Gating strategy of memory T cells.

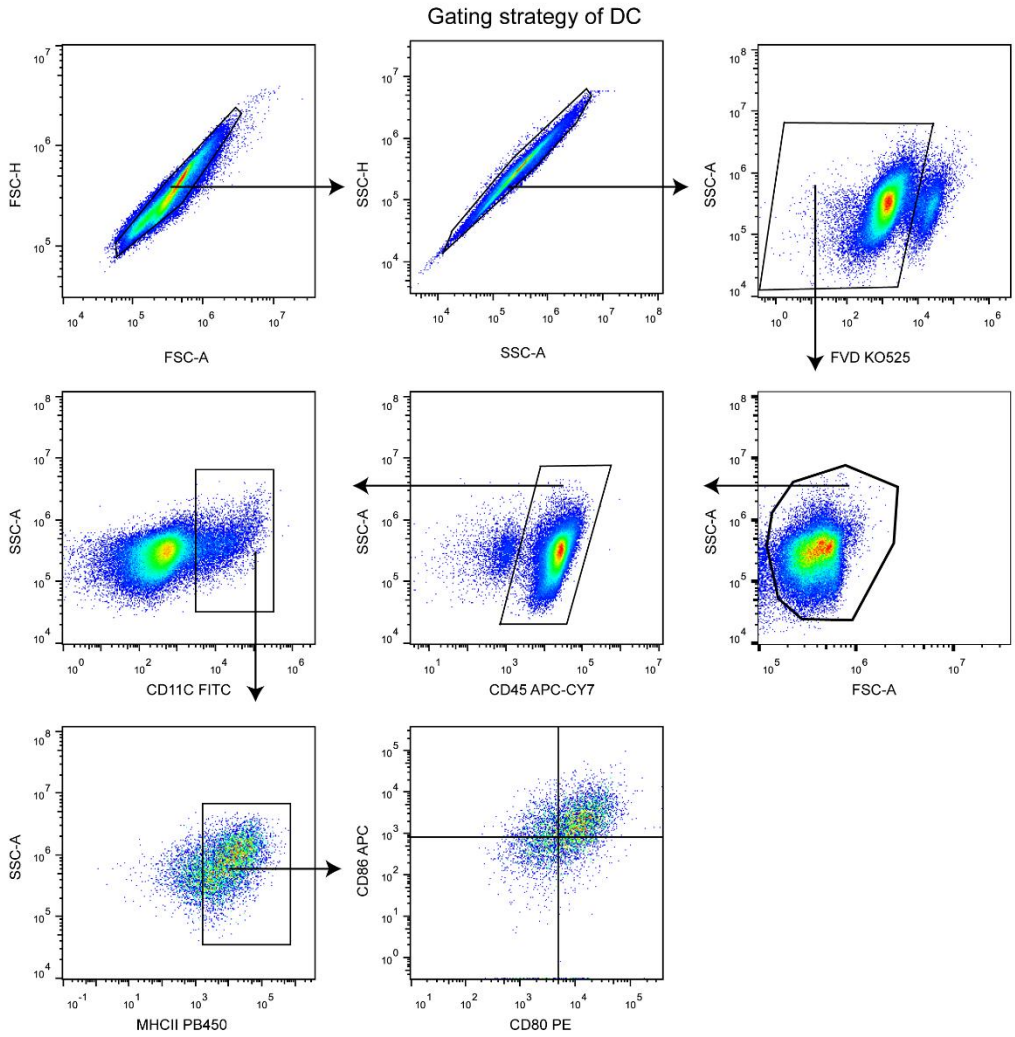

Supplementary Fig. 19. Gating strategy of dendritic cells (DC) in draining lymph nodes (TDLN).

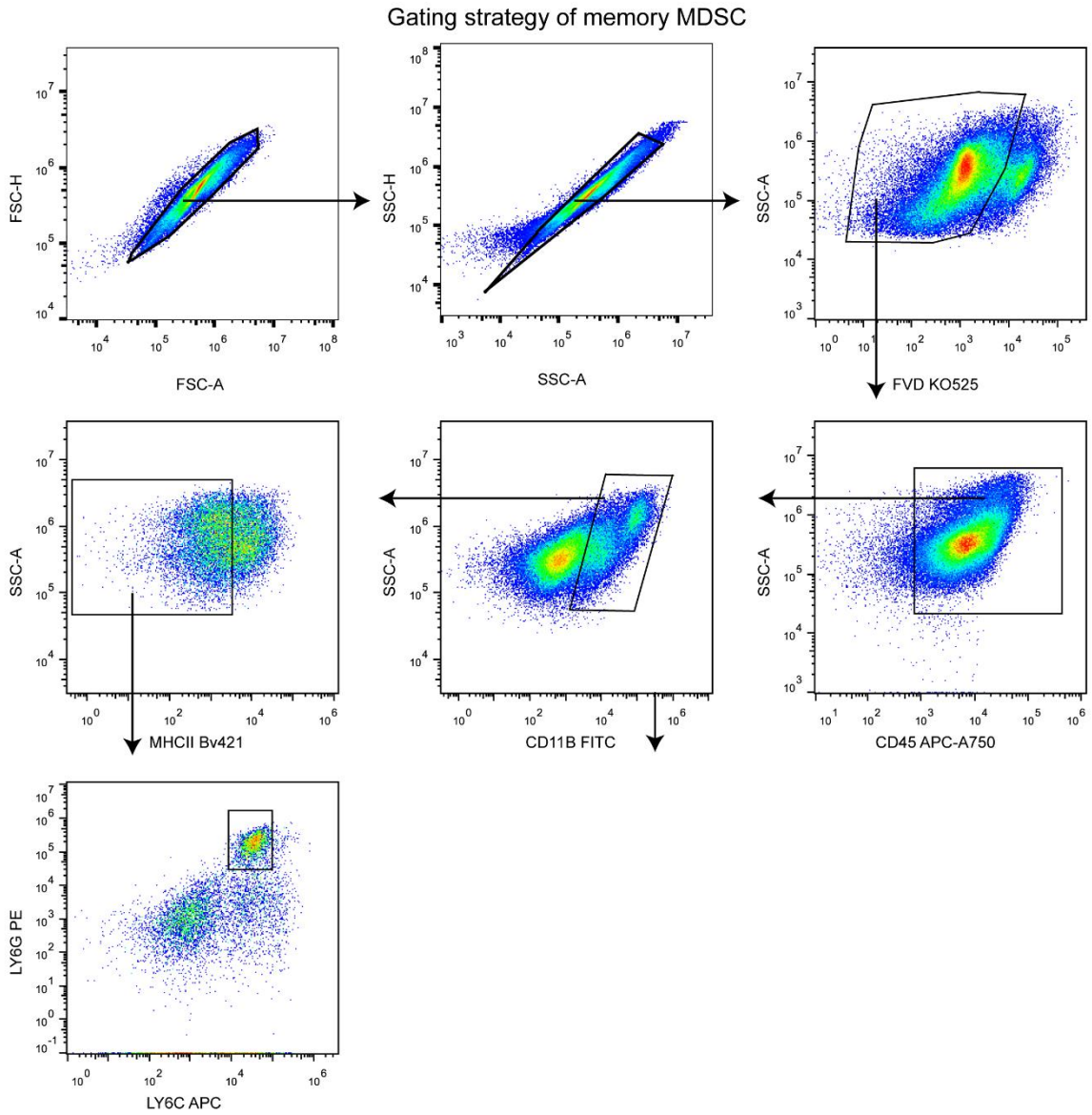

Supplementary Fig. 20. Gating strategy of myeloid-derived suppressor cells (MDSCs) in the spleen.

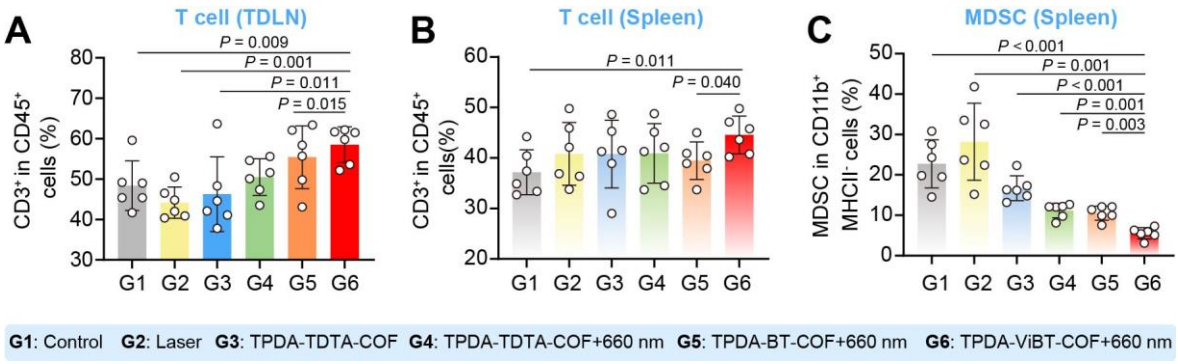

Supplementary Fig. 21. (A) Quantification of T cell ($CD3^+$) gating on $CD45^+$ cells in TDLNs, n = 6 independent samples. (B) to (C) Quantification of T cell ($CD3^+$) gating on $CD45^+$ cells in Spleen, n = 6 independent samples. Quantification of MDSC ($Ly6G^{high}$ $Ly6C^{low}$) gating on $CD11b^+$ $MHCII^-$ cells in the spleen, n = 6 independent samples, $P_{G(3\ vs\ 6)}$ = 5.76E-06. Data are presented as mean ± SEM, statistical significance was assessed using one-way ANOVA with post hoc Tukey test. Source data are provided as a Source Data file.

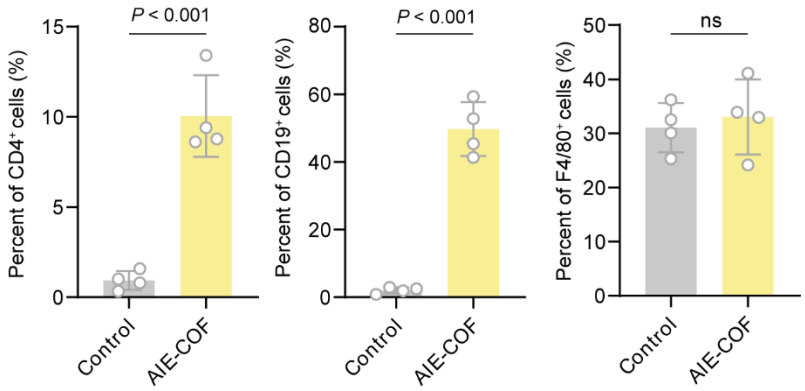

Supplementary Fig. 22. Quantification of mIHC staining of CD4 (green), CD19 (magenta), F4/80 (yellow), and DAPI (blue) in MC38 tumor after and before TPDA-ViBT-COF treatment, n = 4 independent samples, $P_{G(CD4)}$ = 0.0002, $P_{G(CD19)}$ = 2.17E-05. Data are presented as mean ± SEM, statistical significance was assessed using a two-tailed Student's t-test. Source data are provided as a Source Data file.

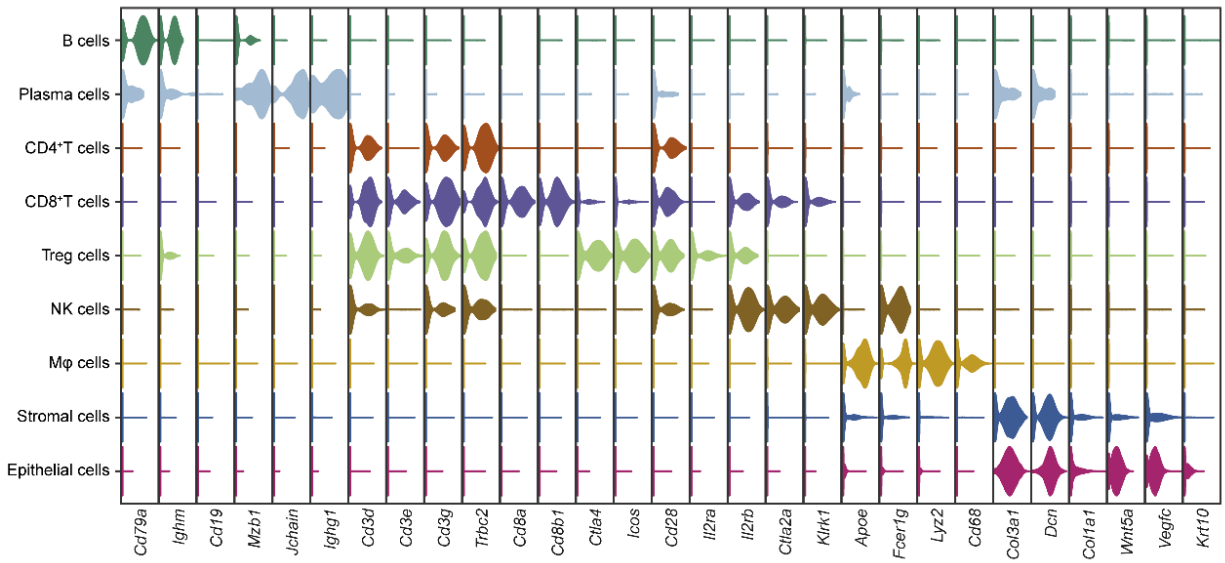

Supplementary Fig. 23. Violin plots show the distribution of expression for marker genes across all cell type clusters.

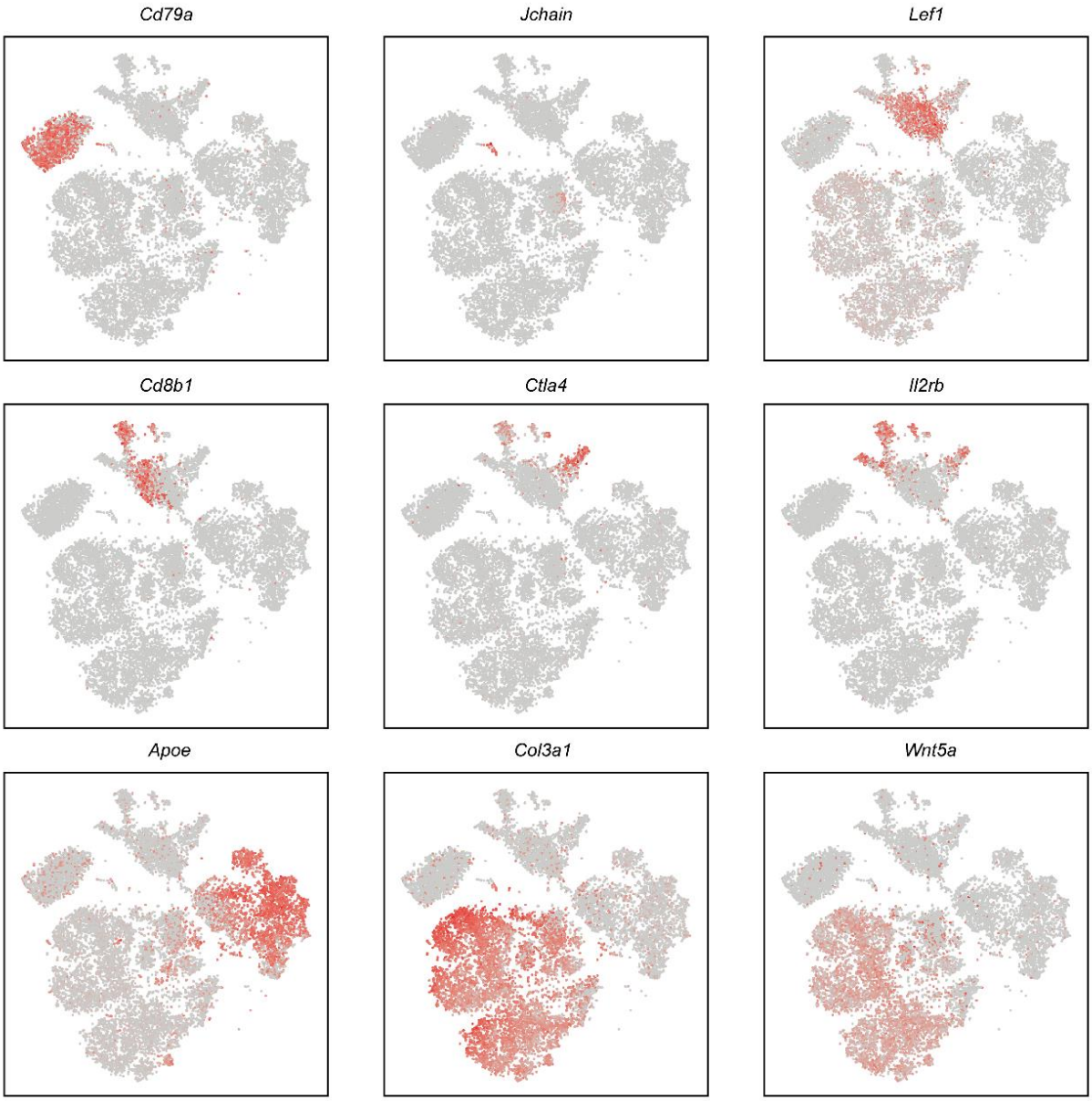

Supplementary Fig. 24. Feature plots show the distribution of expression for marker genes across all cell type clusters.

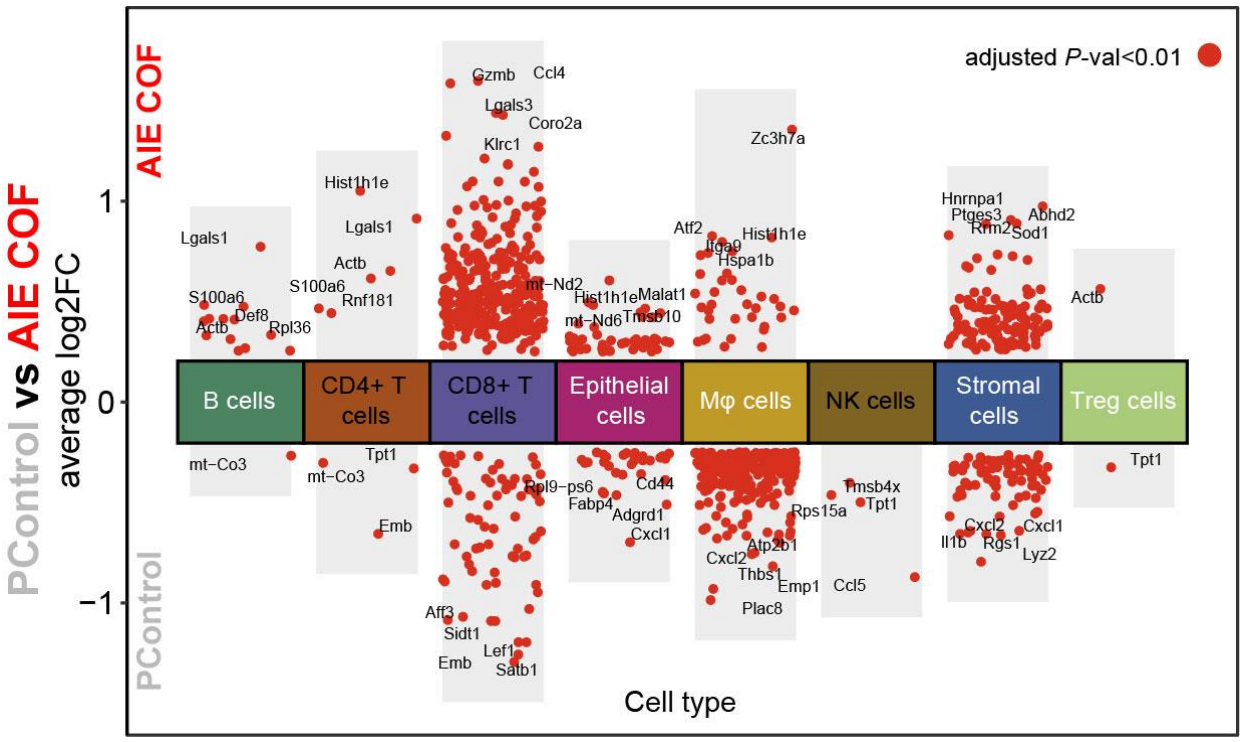

Supplementary Fig. 25. Differential gene expression analysis showing up- and down-regulated genes across all cell types post-TPDA-ViBT-COF treatment. An adjusted *p* value < 0.01 is indicated in red, while an adjusted *p* value R ⩾ 0.01 is indicated in black.

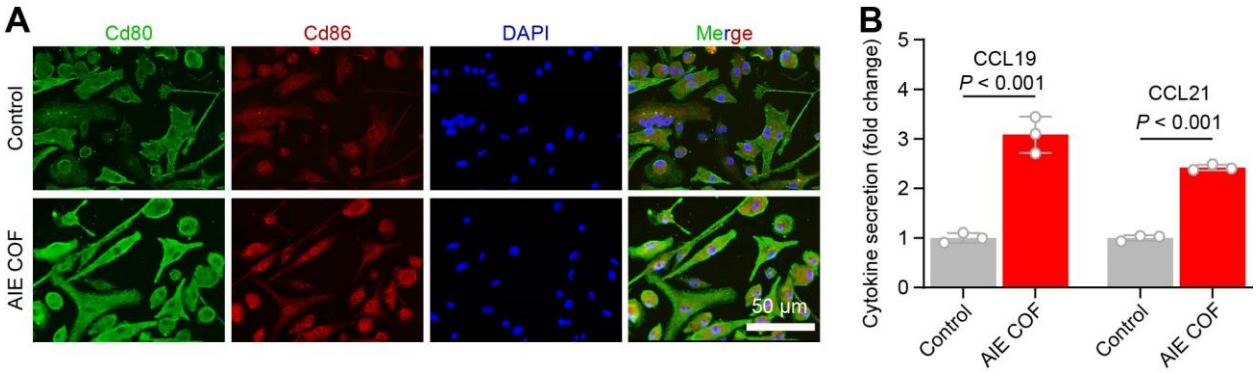

Supplementary Fig. 26. Quantification of the levels of various chemokines in supernatant of primary DCs co-culture with TPDA-ViBT-COF treated MC38 cells. n = 3 independent samples, $P_{G(CCL19)}$ = 0.0006, $P_{G(CCL21)}$ = 3.66E^{-6}, scale bar = 50 μm. Data are presented as mean ± SEM, statistical significance was assessed using a two-tailed Student's t-test. Source data are provided as a Source Data file.

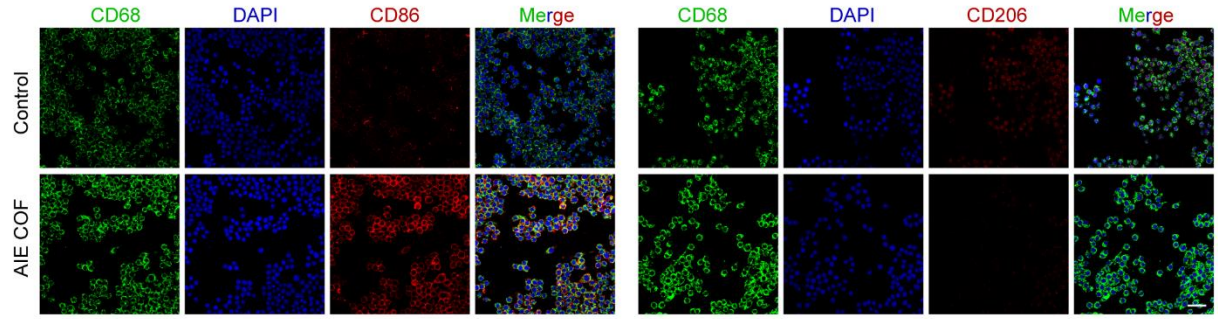

Supplementary Fig. 27. Representative images of CD68, CD86 and CD206 immunofluorescence staining of RAW26.4 cells co-culture with TPDA-ViBT-COF treated MC38 cells, scale bar = 50 μm. Data were repeated thrice independently with similar results.

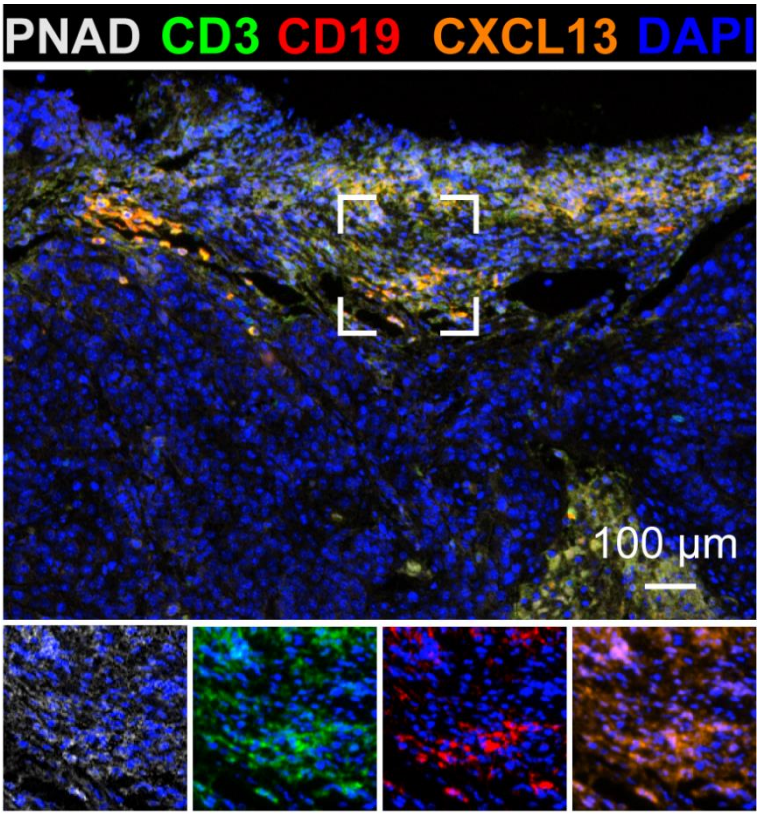

Supplementary Fig. 28. Representative images of mIHC staining of CD19 (red), CD3 (green), PNAD (grey), CXCL13 (orange), and DAPI (blue) in 4MOSC1 tumor with or without TPDA-ViBT-COF treatment. The images at the bottom show the expression of each single marker, with high endothelial venules marker (PNAD), T cells marker (CD3), B cells marker (CD19), and Chemokine marker (CXCL13), scale bar = 100 μm.

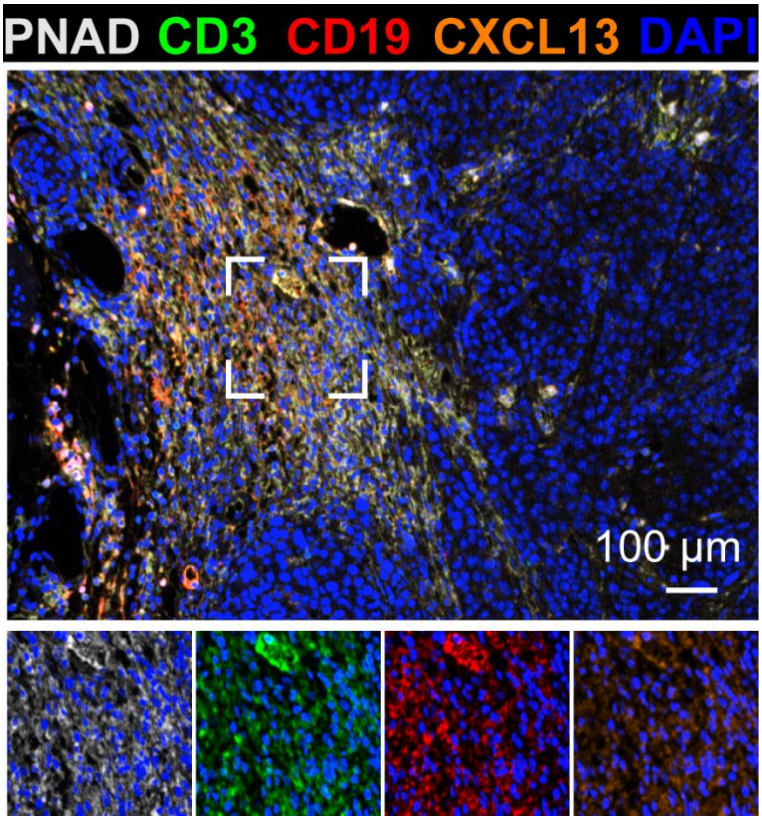

Supplementary Fig. 29. Representative images of mIHC staining of CD19 (red), CD3 (green), PNAD (grey), CXCL13 (orange), and DAPI (blue) in 4MOSC1 tumor with or without TPDA-ViBT-COF treatment. The images at the bottom show the expression of each single marker, with high endothelial venules marker (PNAD), T cells marker (CD3), B cells marker (CD19), and Chemokine marker (CXCL13), scale bar = 100 μm.

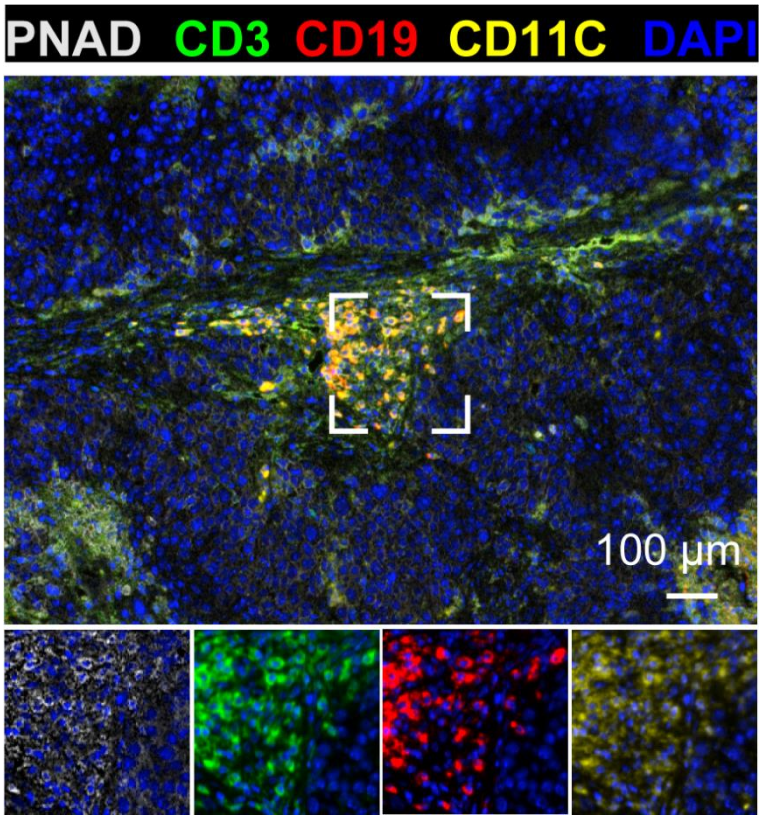

Supplementary Fig. 30. Representative images of mIHC staining of CD19 (red), CD3 (green), PNAD (white), CD11C (yellow), and DAPI (blue) in TPDA-ViBT-COF treated 4MOSC1 tumor. The images at the bottom show the expression of every single marker, with high endothelial venules marker (PNAD), T cells marker (CD3), B cells marker (CD19), and dendritic cells marker (CD11c), scale bar = 100 μm, scale bar = 100 μm.

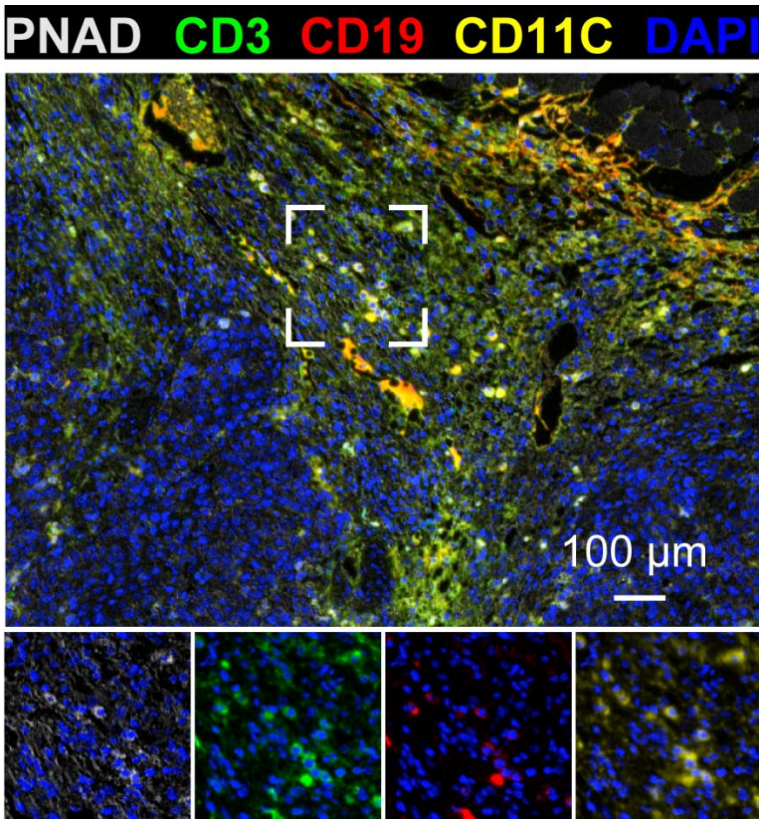

Supplementary Fig. 31. Representative images of mIHC staining of CD19 (red), CD3 (green), PNAD (white), CD11C (yellow), and DAPI (blue) in TPDA-ViBT-COF treated 4MOSC1 tumor. The images at the bottom show the expression of every single marker, with high endothelial venules marker (PNAD), T cells marker (CD3), B cells marker (CD19), and dendritic cells marker (CD11c), scale bar = 100 μm, scale bar = 100 μm.

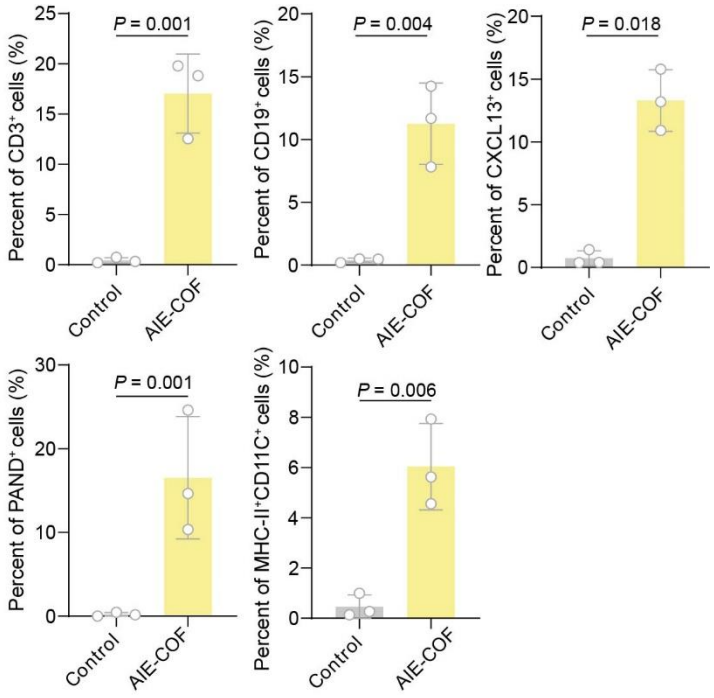

Supplementary Fig. 32. Quantification of CD3, CD19, CXCL13, PAND, and MHCII^{+}CD11C^{+} cells in 4MOSC1 tumor samples that underwent treatment with either control or AIE COF, n = 3 independent samples. Data are presented as mean ± SEM, statistical significance was assessed using a two-tailed Student's t-test. Source data are provided as a Source Data file.

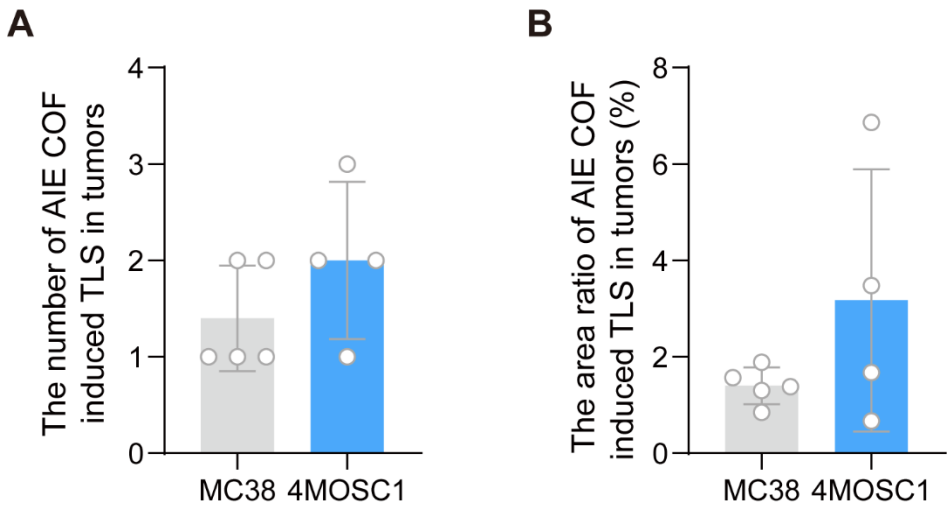

Supplementary Fig. 33. (a) The number of AIE COF-induced TLS in MC38 (n = 5 independent samples) and 4MOSC1 (n = 4 independent samples) tumors. (b) The area ratio of AIE COF induced TLS in MC38 (n = 5 independent samples) and 4MOSC1 (n = 4 independent samples) tumors. Source data are provided as a Source Data file.

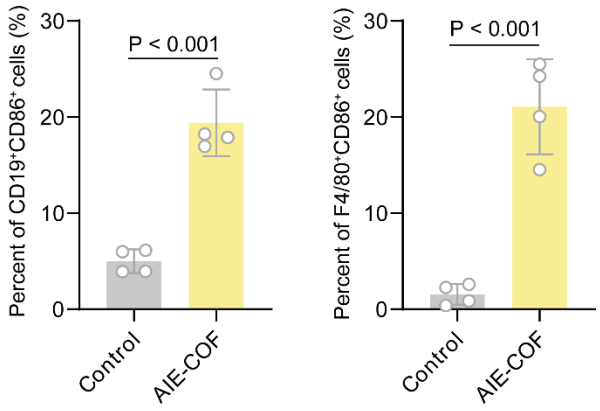

Supplementary Fig. 34. Quantification of $CD19^{+}CD86^{+}$, and $F4/80^{+}CD86^{+}$ in 4MOSC1 tumor samples that underwent treatment with either control or AIE COF, n = 4 independent samples, $P_{G(CD19^{+}CD86^{+})} = 0.0001$, $P_{G(CD19^{+}CD86^{+})} = 0.0002$. Data are presented as mean ± SEM, statistical significance was assessed using a two-tailed Student's t-test. Source data are provided as a Source Data file.

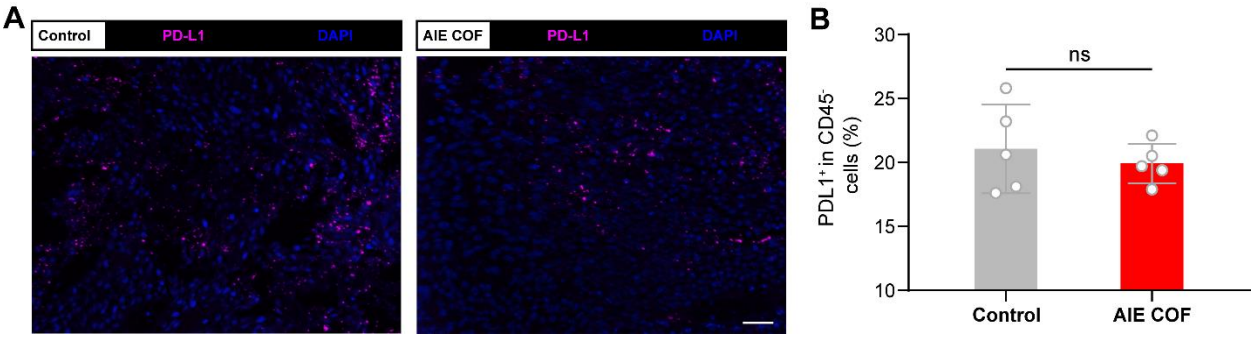

Supplementary Fig. 35. (A) Immunofluorescence images of PD-$L1^{+}$ cells before and after treatment in the tumor, scale bar = 50 μm. (B) Quantification of PD-$L1^{+}$ cells gating on $CD45^{-}$ cells in tumor, n = 5 independent samples. Data are presented as mean ± SEM, statistical significance was assessed using a two-tailed Student's t-test. Source data are provided as a Source Data file.